DUDLEY KNOX LIBRARY
NAVAL POSTGRADUATE SCHOOL
MONTEREY, CALIFORNIA 93943-5002

T232291

NAVAL POSTGRADUATE SCHOOL
Monterey, California

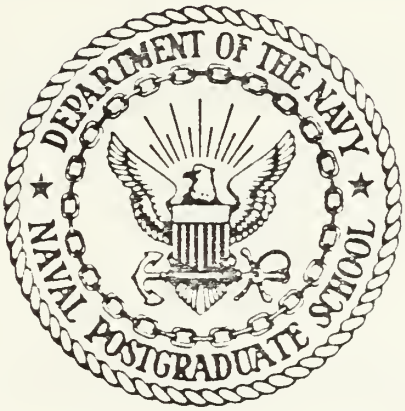

THESIS

WIND FORCING EXPERIMENTS
IN THE
CALIFORNIA CURRENT SYSTEM

by

Philip G. Renaud

December 1986

Thesis Advisor M. L. Batteen
Co-Advisor R. L. Haney

Approved for public release; distribution is unlimited.

REPORT DOCUMENTATION PAGE

1a REPORT SECURITY CLASSIFICATION UNCLASSIFIED	1b RESTRICTIVE MARKINGS
2a SECURITY CLASSIFICATION AUTHORITY	3 DISTRIBUTION / AVAILABILITY OF REPORT Approved for public release; distribution is unlimited
2b DECLASSIFICATION / DOWNGRADING SCHEDULE	
4 PERFORMING ORGANIZATION REPORT NUMBER(S)	5 MONITORING ORGANIZATION REPORT NUMBER(S)
6a NAME OF PERFORMING ORGANIZATION Naval Postgraduate School 6b OFFICE SYMBOL (If applicable) 68	7a NAME OF MONITORING ORGANIZATION Naval Postgraduate School
6c ADDRESS (City, State, and ZIP Code) Monterey, California 93943-5000	7b ADDRESS (City, State, and ZIP Code) Monterey, California 93943-5000
8a NAME OF FUNDING / SPONSORING ORGANIZATION 8b OFFICE SYMBOL (If applicable)	9 PROCUREMENT INSTRUMENT IDENTIFICATION NUMBER
8c ADDRESS (City, State, and ZIP Code)	10 SOURCE OF FUNDING NUMBERS PROGRAM ELEMENT NO / PROJECT NO / TASK NO / WORK UNIT ACCESSION NO

11 TITLE (Include Security Classification)

IND FORCING EXPERIMENTS IN THE CALIFORNIA CURRENT SYSTEM

12 PERSONAL AUTHOR(S)
Renaud, Philip G.

13a TYPE OF REPORT	13b TIME COVERED	14 DATE OF REPORT (Year Month Day)	15 PAGE COUNT
Master's thesis	FROM _____ TO _____	1986 December	88

16 SUPPLEMENTARY NOTATION

17 COSATI CODES			18 SUBJECT TERMS (Continue on reverse if necessary and identify by block number)
FIELD	GROUP	SUB-GROUP	PE ocean model; coastal jet; California Current System; wind-forcing; Flat-bottom; wind stress curl

19 ABSTRACT (Continue on reverse if necessary and identify by block number)

A high-resolution, multi-level, primitive equation ocean model is used to examine the response of an idealized, flat-bottom, oceanic regime off northern California to steady, equatorward, local wind-forcing during the upwelling season. The model has open boundaries on all but the eastern coastal boundary on which either free-slip or zero-slip boundary conditions are imposed. Time-invariant winds, either with or without a component of wind stress curl, are used as model forcing to spin-up a classical two-dimensional, upwelling-induced

20 DISTRIBUTION / AVAILABILITY OF ABSTRACT ☒ UNCLASSIFIED/UNLIMITED ☐ SAME AS RPT ☐ DTIC USERS	21 ABSTRACT SECURITY CLASSIFICATION Unclassified
22a NAME OF RESPONSIBLE INDIVIDUAL Mary L. Batteen	22b TELEPHONE (Include Area Code) 408-646-3265 22c OFFICE SYMBOL 68Bv

Block 19 - ABSTRACT (continued)

coastal jet and undercurrent. Since no eddies are generated, a stability analysis of the mean flow is conducted which explores both the necessary conditions of mixed (barotropic and baroclinic) instability, through calculations of potential vorticity, and the sufficient conditions for baroclinic instability, through an application of a simple two-layer stability model. Comparisons of model results with observations of the coastal jet in the California Current System indicate that the location and the horizontal and vertical current shear associated with the model coastal jet compare favorably with observations; however the modeled jet is stronger, deeper and wider than the observed jet. Finally, the inclusion of wind stress curl and the zero-slip boundary condition are demonstrated to be important elements in model simulations of the coastal jet.

Approved for public release; distribution is unlimited.

Wind Forcing Experiments in the California Current System

by

Philip G. Renaud
Lieutenant, United States Navy
B.S., United States Naval Academy, 1979

Submitted in partial fulfillment of the
requirements for the degree of

MASTER OF SCIENCE IN METEOROLOGY AND OCEANOGRAPHY

from the

NAVAL POSTGRADUATE SCHOOL
December 1986

ABSTRACT

A high-resolution, multi-level, primitive equation ocean model is used to examine the response of an idealized, flat-bottom, oceanic regime off northern California to steady, equatorward, local wind-forcing during the upwelling season. The model has open boundaries on all but the eastern coastal boundary on which either free-slip or zero-slip boundary conditions are imposed. Time-invariant winds, either with or without a component of wind stress curl, are used as model forcing to spin-up a classical two-dimensional, upwelling-induced coastal jet and undercurrent. Since no eddies are generated, a stability analysis of the mean flow is conducted which explores both the necessary conditions of mixed (barotropic and baroclinic) instability, through calculations of potential vorticity, and the sufficient conditions for baroclinic instability, through an application of a simple two-layer stability model. Comparisons of model results with observations of the coastal jet in the California Current System indicate that the location and the horizontal and vertical current shear associated with the model coastal jet compare favorably with observations; however the modeled jet is stronger, deeper and wider than the observed jet. Finally, the inclusion of wind stress curl and the zero-slip boundary condition are demonstrated to be important elements in model simulations of the coastal jet.

TABLE OF CONTENTS

I. INTRODUCTION 11
A. OBJECTIVES 11
B. MOTIVATION AND BACKGROUND 12

II. MODEL DESCRIPTION 17
A. BASIC MODEL DESCRIPTION 17
1. Model Equations 17
2. Domain Size and Resolution 18
3. Forcing Fields 18
4. Finite Difference Scheme 18
5. Boundary Conditions 19
B. SPECIFIC EXPERIMENTAL CONDITIONS 19
1. Method of Determining the Wind Forcing 19
2. PE Model Surface Thermal Damping 30

III. RESULTS OF WIND EXPERIMENTS 34
A. EXPERIMENTS WITH FREE SLIP BOUNDARY CONDITIONS 34
1. Experiment 1 (Uniform Wind) 34
2. Experiment 2 (Wind with Curl) 40
B. EXPERIMENTS WITH ZERO SLIP BOUNDARY CONDITIONS 47
1. Experiment 3 (Uniform Wind) 47
2. Experiment 4 (Wind with Curl) 54
C. STABILITY ANALYSIS 54

IV. COMPARISON OF MODEL RESULTS WITH OBSERVATIONS 71
A. HISTORICAL NOTES ON THE CALIFORNIA CURRENT SYSTEM 71
B. THE COASTAL JET 72
C. COMPARISONS 73

V. SUMMARY AND CONCLUSIONS 78
A. SUMMARY 78
1. Stability Analysis 78
2. Comparison with Observations 79
3. Effects of Offshore Varying Wind Forcing 79
4. Effects of the Zero-Slip Boundary Condition 80
B. RECOMMENDATIONS 80

APPENDIX : ANALYTIC APPROXIMATION OF UPWELLING TIME SCALE 81

LIST OF REFERENCES 84

INITIAL DISTRIBUTION LIST 86

LIST OF TABLES

1. DEFINITIONS OF VARIABLES USED IN THE MODEL 19
2. VALUES OF CONSTANTS USED IN THE MODEL 20
3. ARRANGEMENT OF VARIABLES IN THE VERTICAL FOR THE TWO-LAYER BAROCLINIC MODEL 64
4. TWO-LAYER BAROCLINIC MODEL RESULTS 66
5. DAMPING RATES FOR VARIOUS WAVELENGTHS IN THE PE MODEL 70
6. STATISTICAL COMPARISON OF MODEL RESULTS WITH OBSERVATIONS OF THE COASTAL JET 74

LIST OF FIGURES

1.1 Study area 13

2.1 Climatological wind stress - June. The inside box outlines the model domain 22

2.2 Same as Figure 2.1 except July 23

2.3 Same as Figure 2.1 except August 24

2.4 Climatological wind stress curl - June. The inside box outlines the model domain 25

2.5 Same as Figure 2.4 except July 26

2.6 Same as Figure 2.4 except August 27

2.7 Wind stress curl 29

2.8 Wind stress 31

2.9 Alongshore component wind 32

3.1 Model initial temperature profile 36

3.2 Initial profile of square Brunt-Vaisala frequency, N^2 37

3.3 V-component inertial oscillations 38

3.4 Schematic of coastal jet formation (from Gill, 1982) 39

3.5 Contours of v-component velocity (top), cm/s and temperature (bottom),°C at day 30 for exp. 1 41

3.6 Same as Figure 3.5 except day 60 42

3.7 Same as Figure 3.5 except day 90 43

3.8 Cross-section of v-component velocity alongshore- and time averaged (days 81-90) experiment 1 - contour interval = 5 cm/sec 44

3.9 Same as Figure 3.8 except temperature contour interval = 1° C 45

3.10 Schematic of Ekman pumping (from Gill, 1977) 48

3.11 Contours of u-component velocity contour interval = 0.5 cm/sec experiment 2 - day 6 49

3.12 As in Figure 3.8 except experiment 2 50

3.13 Normalized alongshore velocity averaged in time, depth, and alongshore experiment 3 52

3.14 Same as Figure 3.13 except experiment 1 53

3.15 Same as Figure 3.8 except experiment 3 55

3.16 Same as Figure 3.8 except experiment 4 56
3.17 Potential vorticity in the CCS (exp. 1) 59
3.18 Same as Figure 3.17 except for the Gulf Stream (from Robinson, 1983) 60
3.19 Cross-stream derivative of potential vorticity experiment 1 62
3.20 Same as Figure 3.19 except experiment 3 63
3.21 Baroclinic instability growth rates for all experiments 67
3.22 Same as Figure 3.21 except shows progression of growth rates for experiment 1 69

ACKNOWLEDGEMENTS

The professional guidance, patience, and support of my co-advisors, Dr. Robert L. Haney and Dr. Mary L. Batteen, have been an essential and invaluable part of this thesis. Dr. Haney introduced me to many interesting subjects with potential for thesis applications; one being his primitive equation ocean model which he graciously allowed me to use and modify. Dr. Batteen permitted me to work with her on an NPS Foundation wind-forcing proposal which helped to channel my efforts towards the results presented in this thesis.

My wife, Janice, deserves much credit in the completion of this thesis due to her loving support throughout. Additionally, her expertise in computer systems was of great assistance.

Finally, I would like to dedicate this thesis to my father, George W. Renaud, who passed away prior to its completion. It was all possible only through his encouragement and endorsement of higher education throughout the years.

I. INTRODUCTION

A. OBJECTIVES

The attainment of sufficient knowledge to adequately simulate observed synoptic-mesoscale features of the California Current System (CCS), and to understand the intricate processes responsible for spatial and temporal variations within the system, is the goal of a numerical modeling effort presently underway at the Naval Postgraduate School in Monterey, California. The ability to predict positions, intensities, circulation patterns, etc. of fronts, undercurrents, eddies and current filaments, given an initial set of observations, could provide invaluable assistance to modern naval operations concerned with boundary current acoustic characteristics and associated naval tactics.

Recently, U.S. Naval battle group tactics have been modified by the predictions of a quasigeostrophic (QG) model developed at Harvard University in conjunction with the Naval Postgraduate School. The QG model is initialized by infra-red satellite imagery and air dropped bathythermograph transects across the Gulf Stream and prominent Gulf Stream meanders and rings. After initialization, the QG model is able to predict oceanic conditions out to approximately one week. Accuracy is further enhanced by daily model updates and in-situ verification procedures. The initial results of this operation look extremely promising and there is potential for expansion to other operating areas of the world. With the ever increasing capabilities of high speed computers, the possibility of using a high resolution Primitive Equation (PE) model in an eastern boundary current regime, for instance, is feasible. The vorticity signature of an eastern boundary current is generally less than that of a western boundary current due to the absence of western intensification, and the observed scale of eddies is also smaller. Additionally, while the Gulf Stream, especially its extension region, is in part an open ocean jet and frontal system, the CCS is very much associated with the coastal upwelling region. This region is characterized by significant horizontal variations in stratification and large (topographically and coastally induced) vertical velocities. For these reasons, a high resolution PE model may be more applicable than a QG model for use in areas such as the California Current region. Other agencies, as well, could greatly benefit from such a predictive model, such as the Coast Guard in search and rescue efforts or agencies involved in oil spill recovery, ocean engineering, resource exploration, and at-sea waste disposal operations.

The intent of this research is to provide a contribution towards understanding the processes responsible for synoptic-mesoscale variability in the CCS. The tool used in this research effort is a ten-level, high resolution PE ocean model with idealized topographic capability. The study region extends approximately 500 km offshore from the west coast of North America, and it spans the California coastline from Point Sur in the south to Cape Blanco in the north (Figure 1.1). The particular realm of interest is the effect of wind forcing in the CCS regime. Previous to this effort, an imposed baroclinic jet, intending to simulate the mean CCS, was used as the forcing mechanism to explore potential instabilities of the mean flow (Batteen *et al.*, 1985). Instability of the mean flow occurred in both flat bottom and topographic experiments. It is believed that wind forcing of the local ocean domain could be an equally important process in the CCS and may provide further insight into the dynamics, kinematics, and energetics of this complex eastern boundary current.

B. MOTIVATION AND BACKGROUND

The question as to how to design a limited series of experiments to study the complex mechanisms governing the eastern boundary current regime is not a trivial one. Implementation of wind forcing in a numerical model must be accomplished in a logical manner. The exact method and design of wind forcing experiments raises many questions. Scientific foresight and results from past wind forcing studies must be intelligently used, especially when confronted with limited computer resources. Procedurally, the most important criteria in the design of wind forcing experiments is probably to include only one potential generating mechanism at a time, making it possible to isolate that effect during the analysis and interpretation phase.

The elimination of bottom topography in initial wind forcing experiments allows the role of wind forcing to be isolated from the possible coupled role of wind forcing with bottom topography. The particular developmental stage of the PE model used in this study is such that it does not presently include the depth-averaged, or barotropic flow, component (although it is in the process of being implemented). It is believed that topographic effects would not be well represented unless the depth-averaged component is included. This does not, however, dismiss the effect of bottom topography as an important mechanism in the CCS. The study of bottom topography should be given great consideration in future development of this numerical model.

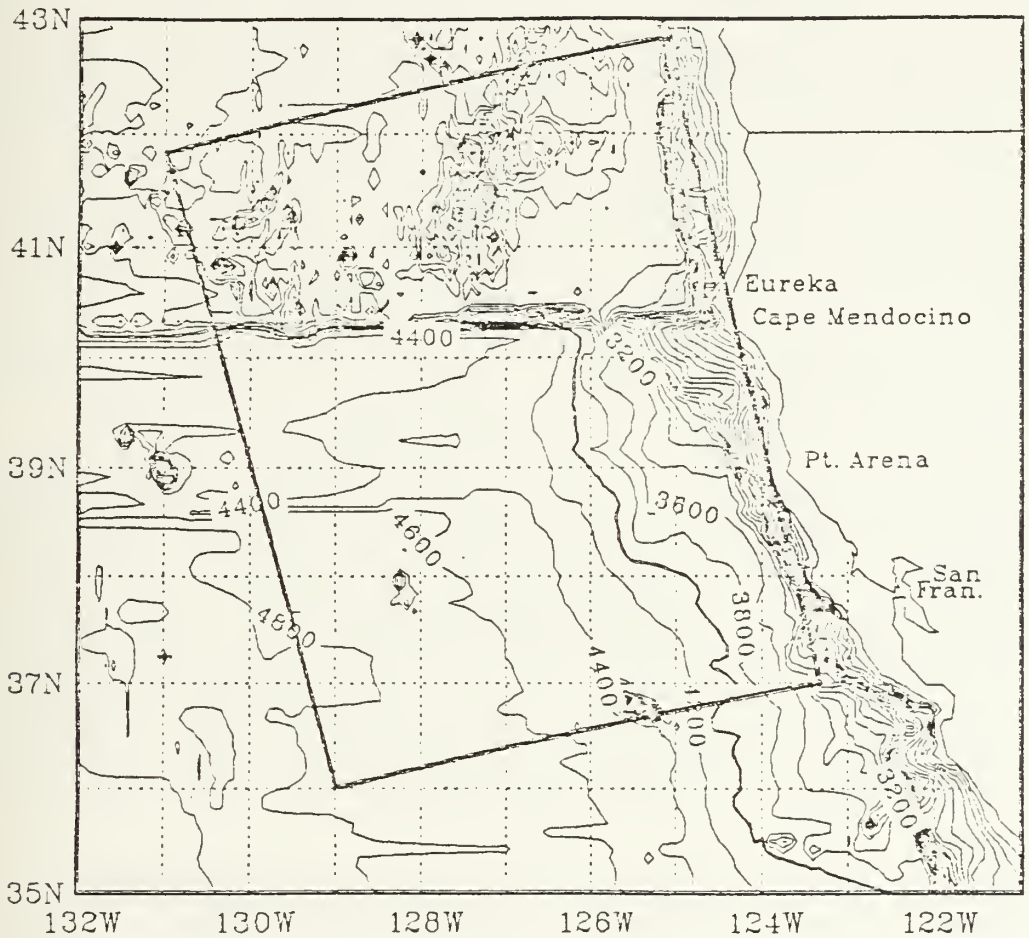

Figure 1.1 Study area.

It is known that local and remote winds drive coastal circulation, the latter by exciting coastal waves (Carton, 1984). Wind-driven coastal upwelling off California is closely tied to the seasonal cycle because northerly winds along the coast, which are favorable for upwelling, are strongest in a climatological sense during summer (Hickey, 1979). Due to the strength of the local winds and the correlation of local winds with upwelling, this study will concentrate solely on the effects of local wind forcing.

Chelton (1984) points out that the detailed temporal and spatial characteristics of the wind field over the California Current are not well known. Probably the most complete description of seasonal winds in the California coastal region is given by Nelson (1977), who compiled direct ship observations in 1° square areas from records dating back to the mid-nineteenth century. Chelton (1984) additionally notes that the spatial structure of the wind field is similar throughout the year but that the magnitude changes seasonally. Although the time dependent nature of winds is an important consideration, it is seen here that an important scale of wind forcing in the CCS region is on the order of a season. Numerical studies to date have considered many different time scales of forcing. Carton and Philander (1984) state that "realistic coastal winds are an essentially random succession of storms with differing scales." Philander and Yoon (1982) consider periodic winds and Carton (1984) describes the coastal response to an isolated storm. This study will focus on the response to forcing at the longest time scale considered to be of importance; that being the seasonal time scale. Shorter time scales are, indeed, interesting and warrant investigation as well. This study will only cover the summer season due to the interest in upwelling mechanisms. Furthermore, because the generation period of eddies (less than a month) observed in the CCS is short compared to the seasonal time scale, the winds will be input as time invariant (steady).

Carton and Philander (1984) discuss that at seasonal time scales, two characteristics of the wind field have been considered as possibly driving the seasonal circulation of the eastern ocean: the alongshore component of wind stress, and wind stress curl. Bryan and Ripa (1978), Hickey (1979), Chelton (1984), and others have suggested that upwelling due to the curl of the wind stress is an important mechanism in establishing pressure gradients. Carton and Philander (1984) conclude that the wind stress curl is important as a forcing function and that it significantly contributes to variability near the coast. Anderson and Gill (1975) and Philander and Yoon (1982) conclude that the alongshore component of the wind stress, which need not contain

any curl, can also contribute to the seasonal variability of the CCS. Chelton (1984) points out that the restriction to a zonally uniform wind stress could be an important weakness of eastern boundary current models because there are strong cross-shore gradients in the wind stress resulting in a nearshore positive wind stress curl. It is seen in the climatological wind record that the winds over the region of the California Current appear to be strongest approximately 200 km offshore so that there is a nearshore positive wind stress curl year round. Additionally, it is noted that the magnitude of this wind stress curl varies seasonally, approximately in phase with the alongshore wind stress. In a recent numerical study on the dynamics of the CCS, McCreary *et al.*, (1986) sought to answer the question of what mechanisms force equatorward flow off the California coast in a region of positive wind stress curl. An important result of that study is that not only the alongshore component of the wind is responsible for the coastal jet but also that the positive wind stress curl is another source of equatorward flow. Obviously, wind stress curl plays a crucial role in the dynamics of the CCS and this study will investigate that effect to some extent.

Another important question which needs to be addressed is whether the solutions are sensitive to the frictional boundary condition, i.e., free-slip or zero-slip, along the rigid eastern boundary of the numerical model. From classical fluid dynamics theory it is expected that the water particles in direct contact with a rigid wall will have zero tangential velocity. This zero-slip condition has greater implications as the resolution of a particular model increases. The PE model used in this study has a zonal resolution of 8 km and the zero-slip condition, therefore, is potentially an important consideration. This is because a uniform long-shore wind stress having no curl will produce vorticity in the ocean near the wall if the condition of zero-slip is used, but no vorticity will be produced if the free-slip condition is used.

In a study of boundary conditions in homogeneous ocean models, Blandford (1971) explored the effect of various boundary conditions (free-slip and zero-slip) in strongly nonlinear flow in a barotropic, β-plane model of the ocean. He found that the solution changes from a steady flow for free-slip to an unsteady flow with the generation of eddies along the western boundary when zero-slip boundary conditions are imposed. This study will compare the effects of free-slip versus zero-slip boundary conditions on the eastern boundary.

With the guidance of important results of past studies, this study of wind forcing of the CCS will focus on local, steady wind forcing of a flat bottom regime with the additional effect of wind stress curl. Also, both free-slip and zero-slip boundary conditions will be explored. The experiments have been designed to proceed in a scientifically logical manner with the purpose of investigating one physical mechanism at a time.

II. MODEL DESCRIPTION

A. BASIC MODEL DESCRIPTION

1. Model Equations

The numerical model used in this study is a ten-level PE model of a baroclinic ocean on an f-plane with no depth-averaged flow (the depth-averaged component is presently being incorporated). The model is based on the hydrostatic and Boussinesq approximations with the rigid lid approximation made. Depth of the model is variable, when idealized bottom topography is used, however, this study will only consider a flat bottom. The governing equations written in sigma coordinates are as follows:

a. Momentum Equations:

$$\frac{du}{dt} = \frac{-1}{\rho_0}\frac{\partial p'}{\partial x} + \frac{1}{\rho_0}\frac{\sigma}{D}\frac{\partial p'}{\partial \sigma}\frac{\partial D}{\partial x} + fv + A_m\nabla^4 u + \frac{K_m}{D^2}\frac{\partial^2 u}{\partial \sigma^2} + \delta_d(u) \qquad (2.1)$$

$$\frac{dv}{dt} = \frac{-1}{\rho_0}\frac{\partial p'}{\partial y} + \frac{1}{\rho_0}\frac{\sigma}{D}\frac{\partial p'}{\partial \sigma}\frac{\partial D}{\partial y} - fu + A_m\nabla^4 v + \frac{K_m}{D^2}\frac{\partial^2 v}{\partial \sigma^2} + \delta_d(v) \qquad (2.2)$$

where $\sigma = z/D$

b. Continuity Equation:

$$\frac{\partial w}{\partial \sigma} + \frac{\partial u}{\partial x} + \frac{\partial v}{\partial y} = 0 \qquad (2.3)$$

c. Vertically Integrated Hydrostatic Equation:

$$p' = D \int^{0}_{\sigma} B \, d\xi - \int^{0}_{-1} [D \int^{0}_{\sigma} B d\xi] \, d\sigma \qquad (2.4)$$

d. Equation of State:

$$B = \alpha \, g \, (T - T_0) \qquad (2.5)$$

e. Thermodynamic Equation:

$$\frac{dT}{dt} = A_H \nabla^4 T + \frac{K_H \partial^2 T}{D^2 \partial \sigma^2} + \frac{1}{D} \frac{\partial}{\partial \sigma} [S(z) - (w'T')] + \delta_d(t) \qquad (2.6)$$

In the above equations, all horizontal partial derivatives are on constant sigma surfaces. In addition, the variables used are defined in Table 1. Other symbols in the model equations are listed in Table 2, which gives values of constants used throughout this study.

2. Domain Size and Resolution

The model domain extends 6° in longitude and 6° in latitude (512 km by 640 km) and has 8 km by 10 km horizontal resolution with ten levels in the vertical. This is the finest horizontal resolution that is practical for use on the IBM 3033 at the Naval Postgraduate School.

3. Forcing Fields

The model can either be spun up from rest or initialized with some known current field, e.g., a baroclinic jet representative of the mean California current. In addition, a surface heat flux, dependent on the model predicted sea surface temperature, can be computed and used to damp the temperature field toward a prescribed climatological value. Details are given below. In this study, the model is spun-up using a representative climatological wind field.

4. Finite Difference Scheme

In the horizontal, a space-staggered B-scheme (Arakawa and Lamb, 1977) is used while a sigma coordinate system controls the vertical. The noisefree version of the hydrostatic equation in sigma coordinates advocated by Arakawa and Suarez (1983) has been implemented.

TABLE 1

DEFINITIONS OF VARIABLES USED IN THE MODEL

SYMBOL	DEFINITION
z	height (positive upwards)
t	time
p′	pressure perturbation from a vertical average
T	temperature
u,v,w	eastward,northward, and vertical (sigma) velocity components, respectively
B	buoyancy
δ_d	dynamic adjustment procedure
S	solar radiation in the ocean
w′T′	turbulent vertical heat flux

5. Boundary Conditions

The northern, western, and southern boundaries are open using a modified version of the radiation boundary condition of Camerlengo and O'Brien (1980). The eastern boundary, representing the west coast of North America, is closed, and straight, with freeor zero-slip capability.

B. SPECIFIC EXPERIMENTAL CONDITIONS

1. Method of Determining the Wind Forcing

The climatological study of Nelson (1977) was used to determine the wind forcing for the PE model domain, which extends from 36.5N to 42.5N and from 124W to 130W (Figure 1.1). Nelson has compiled long-term composite monthly fields of surface wind stress on a 1° square area basis along the west coast of the United States. Nelson states that the monthly mean data described in the report adequately resolves the seasonal cycle, which is the dominant time scale for coastal upwelling (Mooers *et al.*, 1976). Although the PE model is of a finer horizontal resolution (i.e., 8 to 10 km) than Nelson's analysis (approx. 110 km), it is the best data set available for seasonal forcing in the California Current region.

TABLE 2

VALUES OF CONSTANTS USED IN THE MODEL

	VALUE	NAME
Ω	2π day^{-1}	earth rotation rate
C_p	0.958 cal gm^{-1} (°K)$^{-1}$	specific heat of sea water
C_D	1.3×10^{-3}	drag coefficient
L	595. cal gm^{-1}	latent heat of sea water
T_0	278.2 °K	constant reference temperature
ρ_a	1.23×10^{-3} gm cm^{-3}	density of air
ρ_o	1.0276 gm cm^{-3}	density of sea water at T_0
α	2.01×10^{-4} (°K)$^{-1}$	thermal expansion coefficient
K	10	number of levels in vertical
ΔX	$8. \times 10^5$ cm	meridional grid spacing
ΔY	$1. \times 10^6$ cm	zonal grid spacing
D	4.5×10^5 cm	total ocean depth
φ_0	36.5° N	latitude of southern boundary
φ_m	42.5° N	latitude of northern boundary
λ_0	124° W	longitude of eastern boundary
λ_m	130° W	longitude of western boundary
Δt	800. sec	time step
f	0.93×10^{-4} sec^{-1}	Coriolis parameter
g	980.0 cm sec^{-2}	acceleration of gravity
A_M	$2. \times 10^{17}$ cm^4 sec^{-1}	biharmonic momentum diffusion
A_H	$2. \times 10^{17}$ cm^4 sec^{-1}	biharmonic heat diffusion
K_M	0.5 cm^2 sec^{-1}	vertical eddy viscosity
K_H	0.5 cm^2 sec^{-1}	vertical eddy conductivity
P_{sfc}	1013.25 mb	surface air pressure

The choice of selecting a specific span of time over which climatological data would be used was driven by interest in the season most favorable for coastal upwelling in the California Current System, which has been most often observed to occur during the summer (Hickey, 1979). As a result, the months of June, July, and August were chosen for the experimental time domain for this study.

Close inspection of Nelson's climatological data over the model's region during the summer months, Figures 2.1 through 2.3, shows a large variability in the surface stress field in the offshore direction, and little variability in the alongshore direction. As a result, it was decided to use an idealized alongshore wind stress only, and to make it a function of the offshore direction only.

A geographical interpretation problem arises from the fact that the PE model has a straight coastline. The climatological data, of course, is based on the actual position of the California coast, which is not straight. Furthermore, as Figures 2.4 through 2.6 show, the wind stress curl has a strong dependence on distance from the coast. A simple mapping of data from the actual shape of the coast to the straight model coast was performed to partly model the effect that the actual coast has on values of wind stress curl.

The reason for exercising care in the preservation of a realistic pattern of wind stress curl is that wind stress curl is the forcing function for the vertically integrated mass transport of the wind-driven ocean circulation (Nelson, 1977). More importantly, horizontal variations in mass transport in the surface (Ekman) layer produce surface divergence (convergence) corresponding to positive (negative) wind stress curl. The Ekman pumping velocity resulting from the divergence is approximately (ρf^{-1}) times the curl of the wind stress (Gill, 1982). Ekman pumping can significantly contribute to, and modify, the coastal upwelling regime.

Another general observation of Nelson's wind stress data is that the wind stress vectors during the months of June, July, and August, over the model domain, are parallel to the coast within about 10-20% accuracy. This means that the magnitude of wind stress vectors represents, to approximately 80-90% accuracy, the alongshore component of surface stress. Since the PE model's coastline is oriented due north and south, the observed alongshore component is assumed to coincide with the model's north component of surface stress. This observation led to the decision to use the magnitude of Nelson's wind stress as the north component of the model stress. The zonal (cross-shore) component of the model stress is taken to be zero in all experiments.

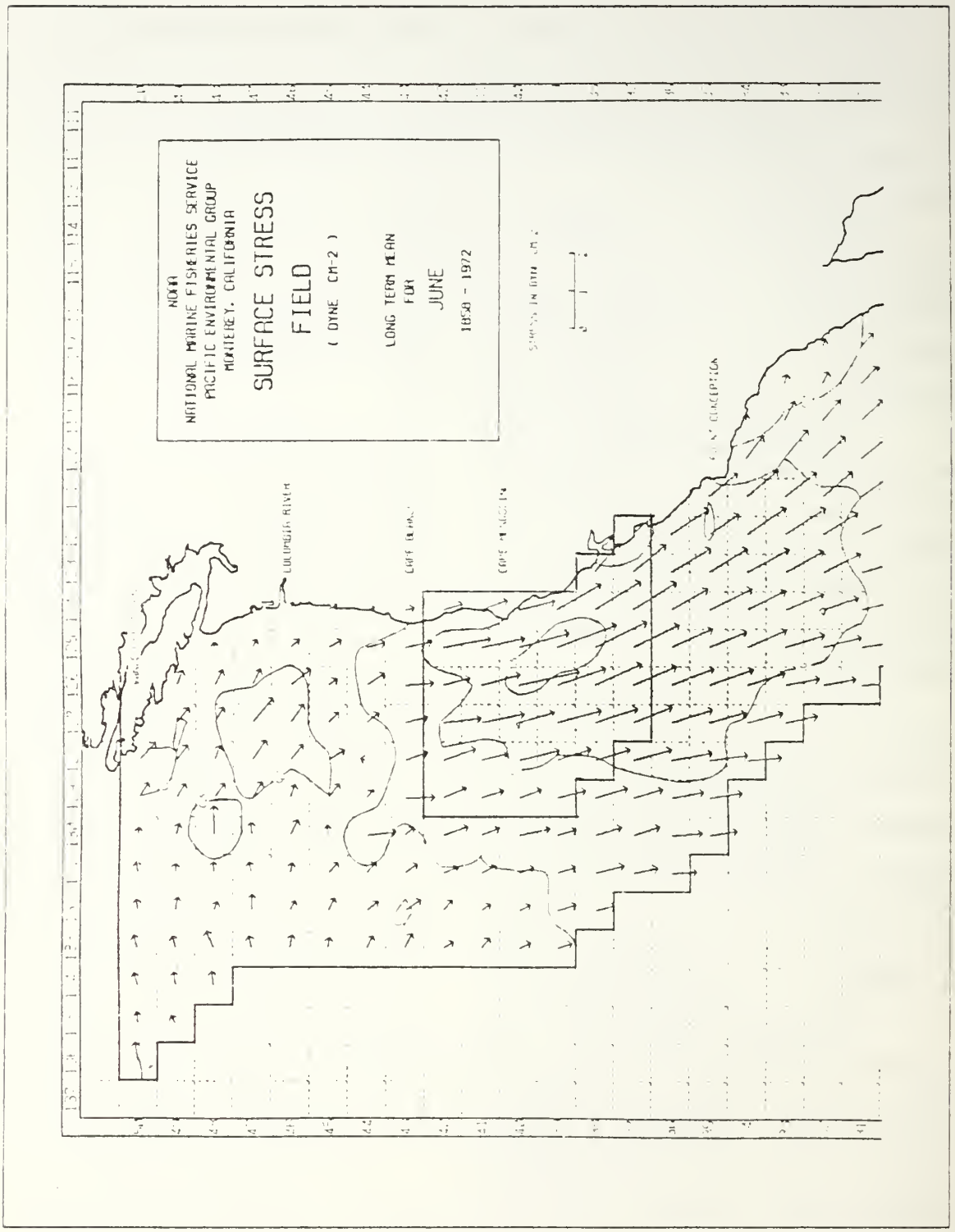

Figure 2.1 Climatological wind stress - June.
The inside box outlines the model domain.

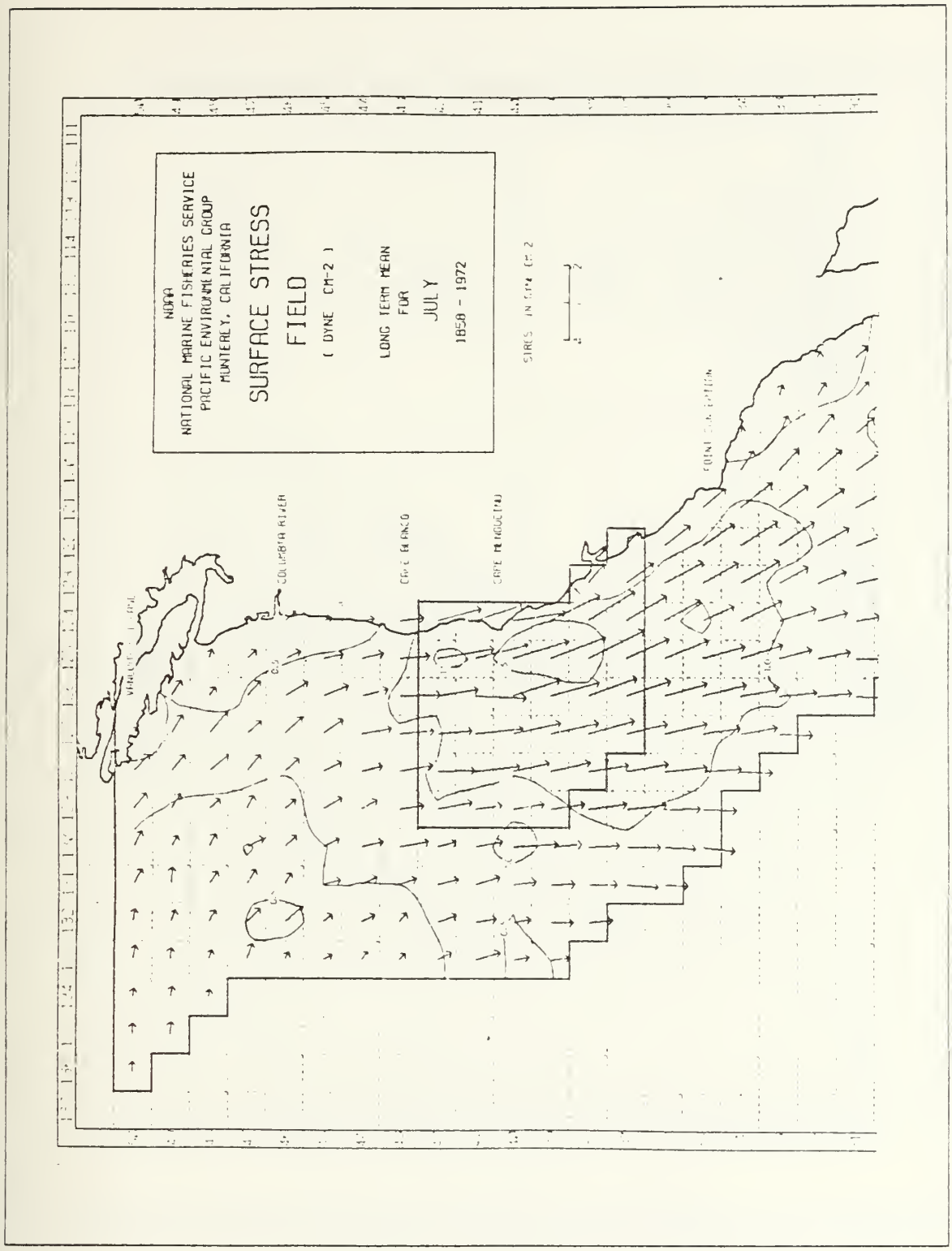

Figure 2.2 Same as Figure 2.1 except July.

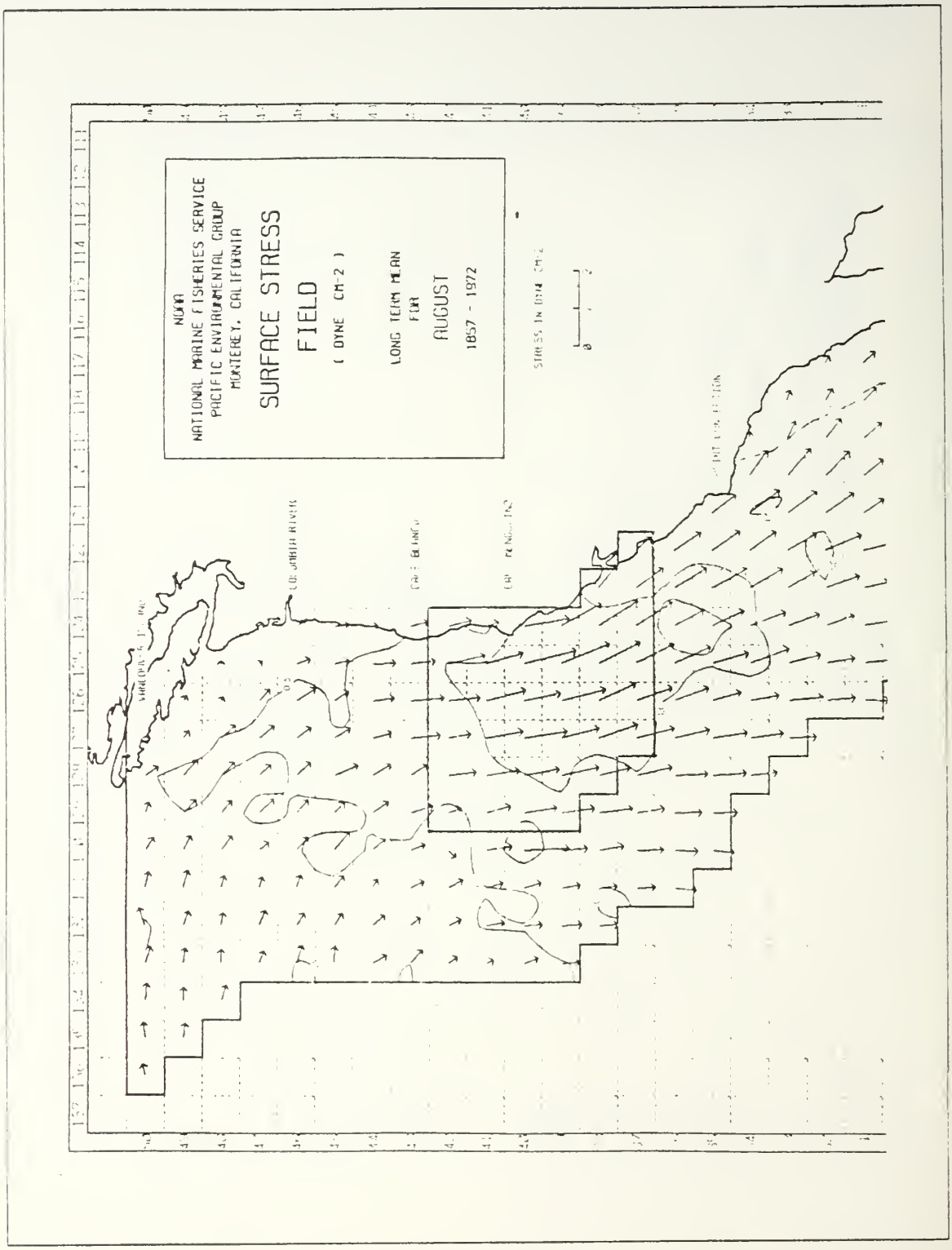

Figure 2.3 Same as Figure 2.1 except August.

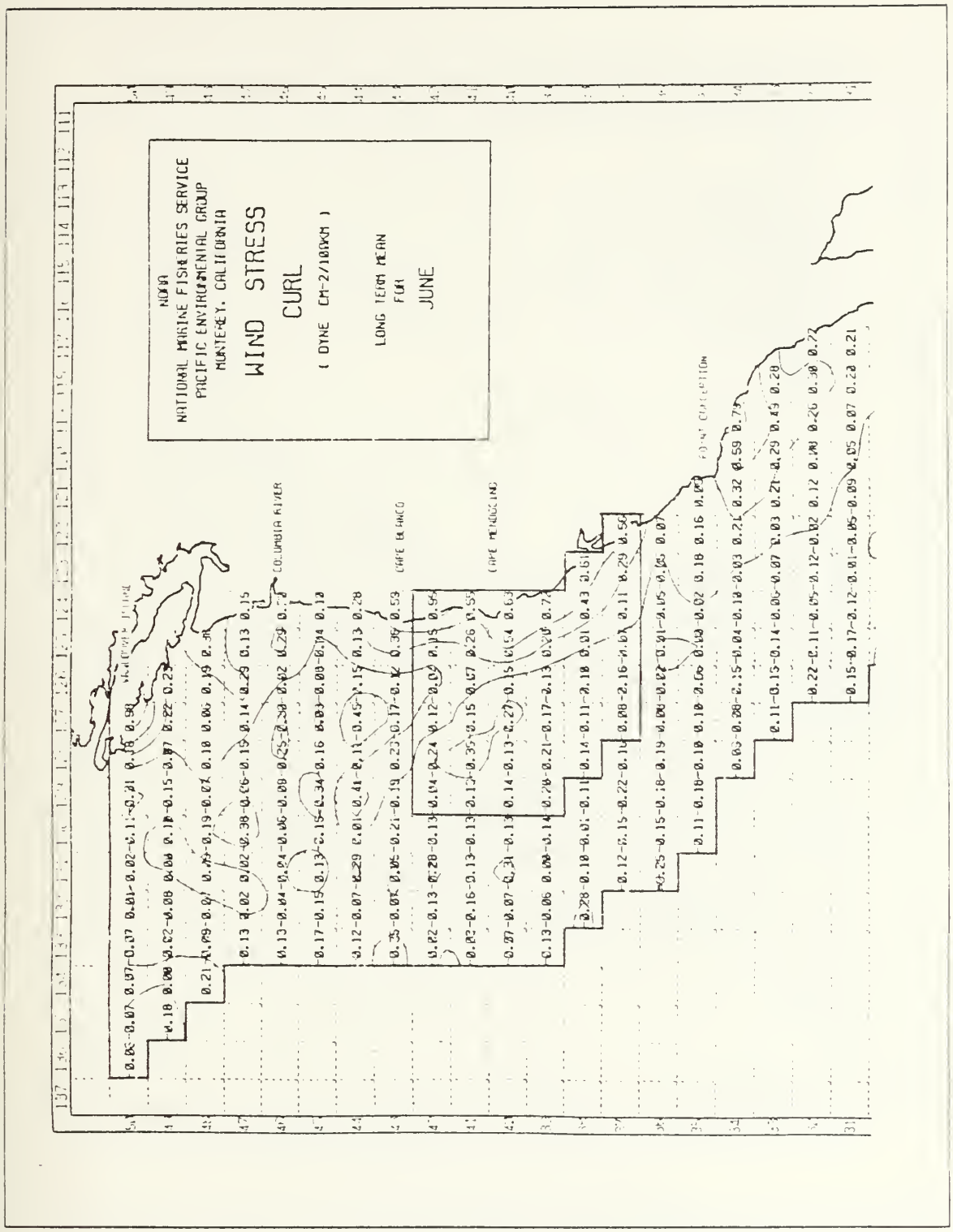

Figure 2.4 Climatological wind stress curl - June.
The inside box outlines the model domain.

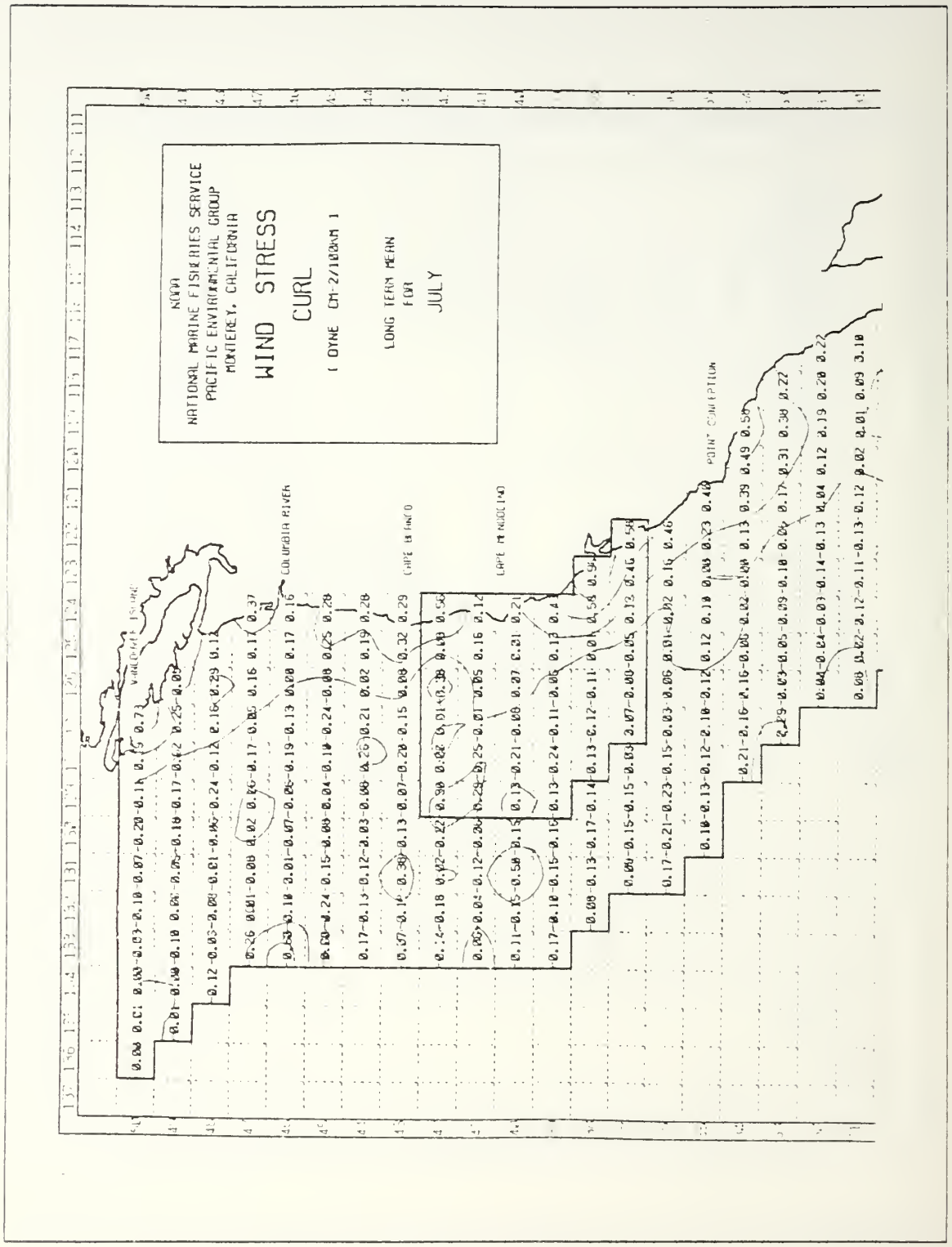

Figure 2.5 Same as Figure 2.4 except July.

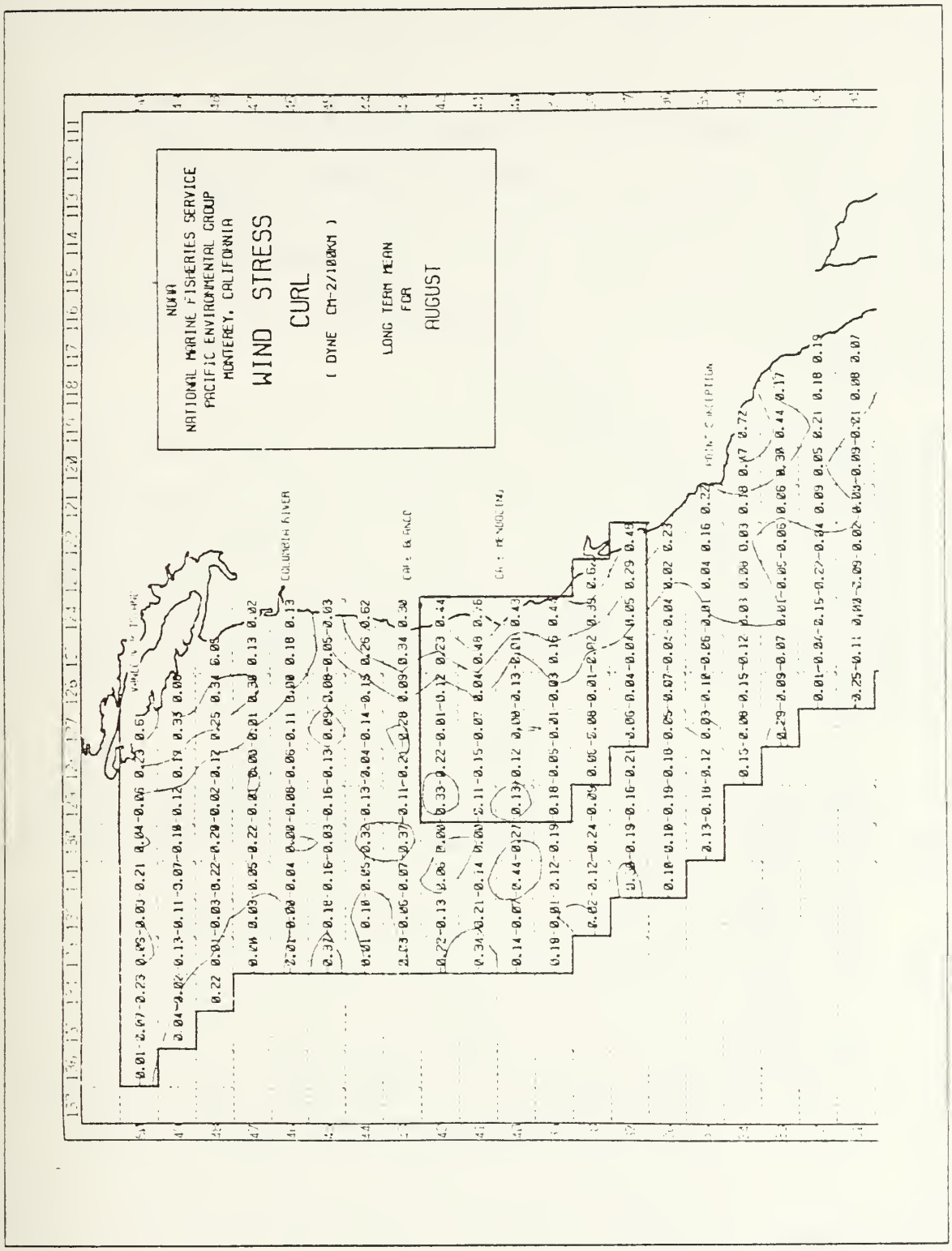

Figure 2.6 Same as Figure 2.4 except August.

For each month in consideration, a total of 36 data points were extracted from Nelson's data set for both wind stress and wind stress curl because the domain of the PE model spans 6° of latitude and 6° of longitude and Nelson's data is of a 1° resolution. Since the alongshore variation was considered much less significant than the cross-shore variation for both wind stress and wind stress curl, an alongshore average of the wind stress curl was calculated from Figures 2.4 through 2.6 and then averaged over the three months of June, July, and August. The result is shown by the circles connected by a dotted line in Figure 2.7. The dominant feature is a region of strong positive curl within 200 km of the eastern boundary, and weaker negative curl over the outer 300 km. This time-averaged and alongshore averaged curl reaches its maximum value at the eastern boundary.

The modeling effort for producing an idealized wind forcing function was based on understanding that the wind stress curl is a prominent feature which will produce a modifying effect on the dynamics of ocean circulation. The observed three-month average, alongshore-averaged wind stress curl, derived from Nelson's climatology (Figure 2.7), was closely examined for features which could be represented by an analytical function. A Gaussian function in the offshore coordinate was found to fit the climatological data satisfactorily. The Gaussian function used to represent the observed curl is:

$$\partial\tau/\partial x = 0.77\exp[-0.5(XR/95.0)^2) - .11 , \qquad (2.7)$$

where XR is distance offshore in kilometers. Figure 2.7 shows a plot of this analytical function (square boxes connected by a solid line) along with the observed values, and the fit is seen to be quite good.

The PE model is designed to use wind input (for convenience of wind stress and heat flux computations) rather than wind stress curl, but in order to benefit from a realistic wind stress curl function and also retain the ability to force the PE Model with wind data, idealized wind data were derived from the above Gaussian representation of wind stress curl in the following manner. The first step was to calculate the value of the wind stress curl (at each u,v gridpoint) using the Gaussian function in Figure 2.7. Next, to compute the surface stress (at the temperature gridpoints) from the wind stress curl (at each u,v gridpoint), the wind stress curl was numerically integrated in the offshore direction. The constant of integration was obtained from the alongshore and three-month average of the data from Nelson (1977). This constant is $\tau_y = -0.65$

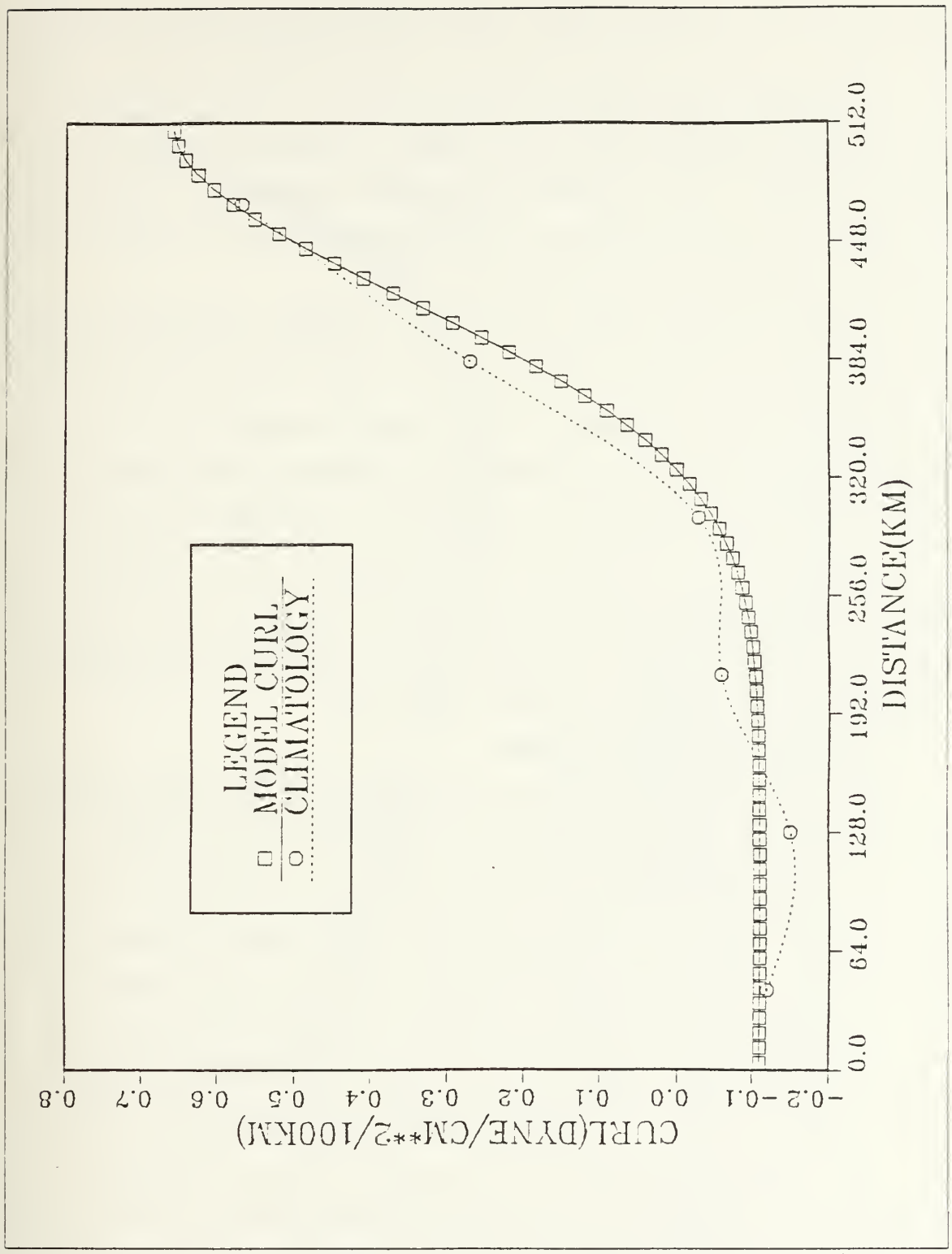

Figure 2.7 Wind stress curl.

dyne/cm^2 and it represents the value of the alongshore wind stress at the coast. The final step in deriving winds from the idealized stress was to utilize the bulk aerodynamic formula to compute winds at model temperature gridpoints. A constant drag coefficient of 0.0013 was utilized with an air density of 0.00123 gm cm^3. Wind values were defined at model temperature gridpoints because the surface wind speed is used in heat budget calculations within the PE model, and therefore it is needed at each temperature gridpoint. Upon completion of heat budget calculations, the PE model computes the wind stress and performs a four-way averaging to get the stress at each u,v gridpoint, whereupon it drives model surface currents.

A plot of the wind stress, obtained by integration of the idealized curl function, is shown by the squares in Figure 2.8. It is clear that the proper shape and order of magnitude has been captured well. Any difference between modeled and climatological wind stress is probably due to the modeling assumption that the curl is determined solely by the offshore variation of the alongshore stress. A plot of the alongshore component of the winds computed from the observed and modeled stress, respectively, using the bulk aerodynamic formula, is shown in Figure 2.9. Again, the shape and magnitude is well represented and any differences are just reflections of differences in the wind stress plots. This idealized wind (having the stress and stress curl as shown in Figures 2.8 and 2.7 respectively) is the actual data which was used to force the PE model in some of the wind forcing experiments.

2. PE Model Surface Thermal Damping

Surface thermal damping becomes a crucial requirement for realistic modeling of ocean temperature fields in the presence of atmospheric surface wind forcing. This is because the summer heat flux in the California region is a downward flux due to a greatly reduced sensible and latent heat flux produced by the existence of cold (upwelled) water. The stronger the alongshore (southward) winds, the greater the upwelling and the colder the surface water and the greater the downward heat flux. The downward heat flux is thus negatively correlated with the sea surface temperature, hence it is a damping factor. Another way to understand the damping (as contrasted to forcing) nature of the surface heat fluxes in the CCS is to recognize that the largest downward surface heat fluxes occur where the ocean surface temperatures are the coldest. Heat flux variations related to atmospheric variations in clouds or air temperature are not considered to be an important forcing factor in the CCS. Heat fluxes are therefore computed from bulk formulae using prescribed quantities of

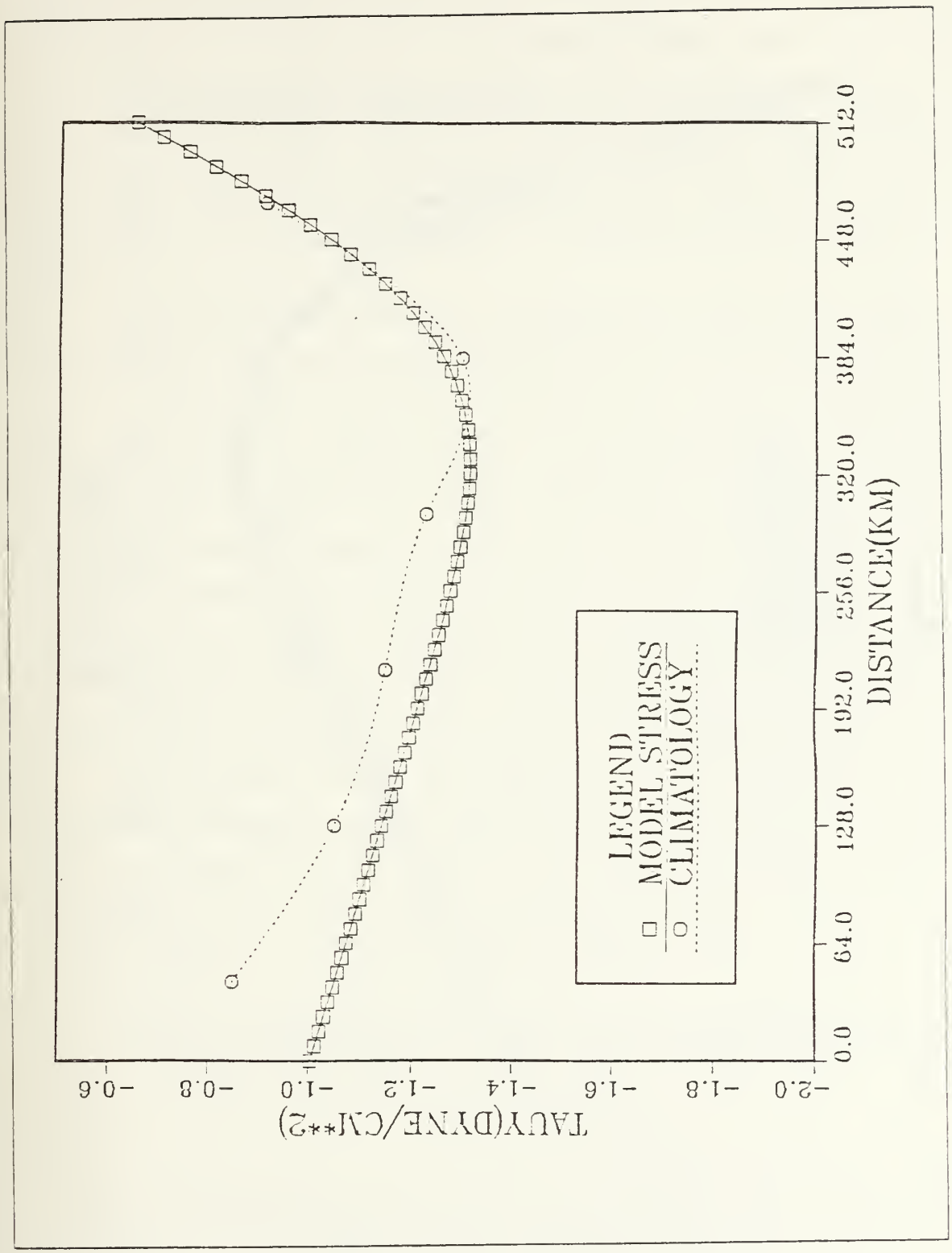

Figure 2.8 Wind stress.

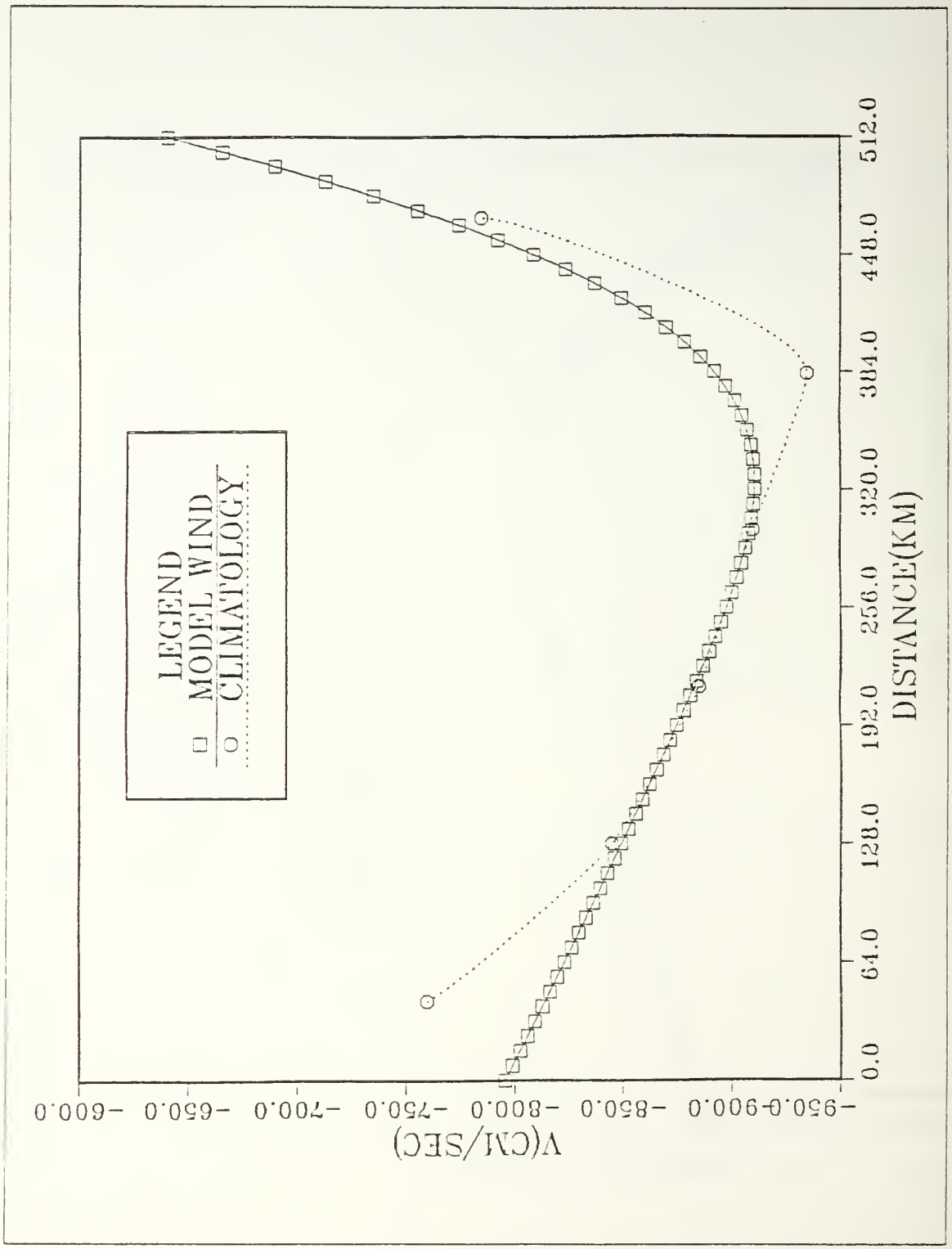

Figure 2.9 Alongshore component wind.

atmospheric solar radiation, clouds, surface air temperature, relative humidity and winds (Haney *et al.*, 1978). The following representative mean values, for the summer season, are used: fractional cloud coverage of 48%, solar insolation at top of the atmosphere of 983.3 cal/cm^2/day, and surface relative humidity of 85%. The value of solar radiation was obtained from the Smithsonian Meteorological tables (List, 1963), the fractional cloud cover was obtained from the satellite cloud atlas of Miller and Feddes (1971), and the relative humidity was computed from climatological data of Nelson (1983).

Sensible and latent heat fluxes are calculated using exchange coefficients which are proportional to the wind-speed-dependent neutral drag coefficient [$C_d(V)$] of Large and Pond (1981). Initial conditions for sea surface and air temperatures, respectively, are 15° C sea surface temperature and 13° C air temperature. The sea surface temperature used is a representative offshore temperature for the summer, whereas the air temperature was chosen so that there would initially be no net heat flux at the surface with a steady wind speed of ~ 850 cm/sec (wind speed used for experiment 1). The imposed criteria of no initial heat flux guaranteed that any heat flux generated after model initialization was only in response to the changing sea surface temperature. This criteria also assured that the model heat budget acted only to thermally damp the effects of surface wind forcing and not as an additional forcing function. This is not only realistic, as noted above, but it also simplifies the interpretation later.

The damping nature of the computed heat flux is demonstrated best by considering a linearized form of the modeled equations for the total downward surface heat flux, Q, which is $Q = \gamma(TA^{*}\text{-}SST)$. TA^{*} is an apparent atmospheric equilibrium temperature, SST the model surface-layer temperature and γ a coupling coefficient strongly dependent on surface wind speed, (Haney, 1985). The corresponding relaxation time for the surface temperature is given by $\lambda^{-1} = \rho C_p h \gamma^{-1}$ (Haney, 1985), where ρ is the density of sea water, C_p the specific heat of sea water, and h the depth of the mixed layer. With mean climatological winds, $\gamma \sim 25 Wm^{-2}K^{-1}$ (Haney, 1971). Using h = 50m, a value is obtained for λ^{-1} of 100 days. Since γ is directly proportional to wind speed, if the wind speed changes on the order of 20%, the temperature relaxation time will also change by 20% yielding a range for λ^{-1} of 80 to 120 days. This long damping time will not mask any change in ocean temperature due to dynamical processes which are expected to have a time scale of only several days.

III. RESULTS OF WIND EXPERIMENTS

A. EXPERIMENTS WITH FREE SLIP BOUNDARY CONDITIONS

1. Experiment 1 (Uniform Wind)

In the first experiment conducted, the idealized winds obtained from the procedure described in Chapter II, and shown in Figure 2.9, were averaged in the cross-shore direction resulting in a constant value (approximately 850 cm sec). The forcing for experiment 1 was, therefore, uniform (alongshore and cross-shore invariant) and steady (time invariant). This idealized wind was considered to be the least complex; yet it still retains some of the realism of observed, long-term, mean climatological winds during the summer season over the geographical region encompassed by the PE model domain. All experiments in this study, unless otherwise stated, included surface thermal damping as described in Chapter II. Additionally, the eastern boundary (representing the west coast of North America) was set as a free-slip condition in this experiment, meaning that the tangential ocean velocities were unrestricted by frictional effects.

At this time, it is important to discuss the initial conditions, in particular the model temperature stratification for the wind forcing experiments. A pure exponential temperature profile, as a function of height (z), was used to initialize all of the experiments within this study. This profile has a length-scale of 450 m with a temperature at the first sigma level (ocean surface level) of 15° C and a value at great depth of 2° C. The exact form of this temperature function is as follows:

$$T(z) = 2 + 13\, e^{z/450}. \qquad (3.1)$$

The temperature profile was derived from observations used to support the Princeton Dynalysis model (Blumberg *et al.*, 1984) and is representative of the long-term, mean climatological temperature stratification for the California coastal region. Additionally, the Brunt-Vaisala frequency profile, $N^2(z)$, was calculated analytically using the temperature function in (3.1) from

$$N^2 = \alpha\, g\, \partial T / \partial z. \qquad (3.2)$$

The model temperature profile and resultant N^2 profile are shown in Figures 3.1 and 3.2. Since the initial temperature field was horizontally uniform, the initial ocean currents were set to zero.

The model was spun up by turning on the wind, at model time zero, to its full magnitude. The impulsive wind produced an impulsive surface stress which resulted in inertial oscillations of the near-surface ocean currents. These oscillations are demonstrated by a time series of the v-component of velocity at a selected gridpoint away from the coast (Figure 3.3). The inertial period approximated from Figure 3.3 of $\sim$ 0.75 day compares well with the theoretical inertial period of 2π f. Off-shore Ekman transport was apparent from the negative values of the u-component of velocity throughout the model spin-up (see Figure 3.11). Since the wind was northerly, and the model domain is in the northern hemisphere, Ekman transport was directed to the right of the direction of the surface stress; which is towards the west (represented by negative values of the u-component of velocity). The Ekman flow away from the rigid eastern boundary produces some very important effects. Water carried seaward, in the oceanic boundary layer, produces divergence at the coast. Due to the principle of conservation of mass, the void created by coastal divergence must be filled by upwelling of colder water from lower levels.

The effect of upwelling, which brings colder water up from the lower levels, is to perturb the initial, horizontally uniform, temperature structure. The isotherms are bent upward near the coast, which establishes a horizontal temperature gradient in the upper levels of the water column. The vertical velocities established by upwelling in the PE model compare favorably with an analytical approximation of upwelling rates using basic principles and assumptions (see Appendix). Consistent with geostrophy (a balance between the pressure gradient force and the Coriolis force) and the resulting thermal wind equations (a relation of vertical shear to the horizontal temperature gradient), the model spin-up is characterized by a coastally-trapped, alongshore jet in the upper 1000 m of the water column. A simple schematic of the coastal jet is shown in Figure 3.4 from Gill (1982). The southward flowing jet along the eastern boundary of the model domain will be the focal point of this study.

Figures 3.5 through 3.7 show contours of the v-component of surface velocity, along with contours of temperature, during the spin-up phase at days 30, 60, and 90 respectively. The coastal jet develops in response to the increase in the horizontal temperature gradient with time. The near-coast, surface, horizontal temperature

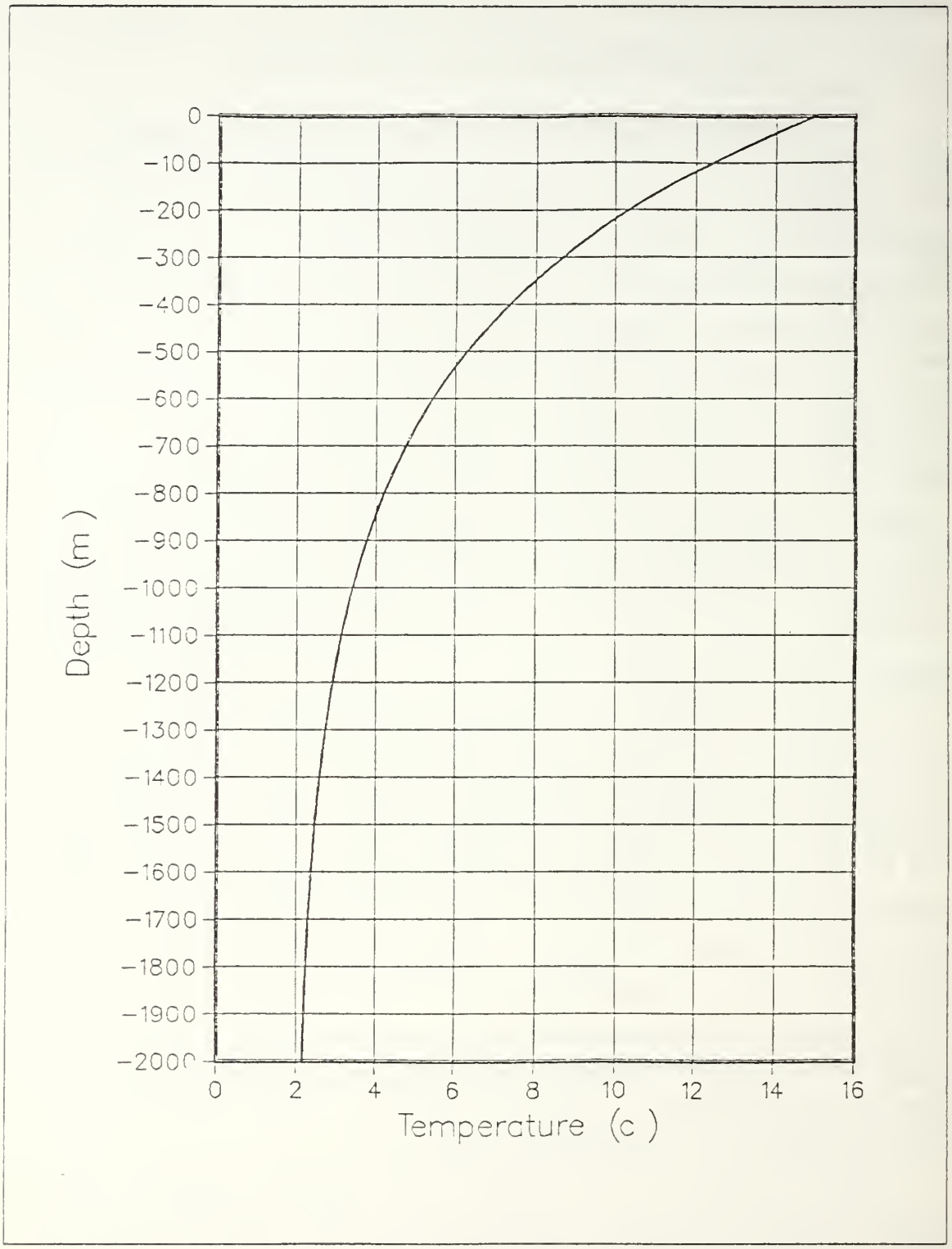

Figure 3.1 Model initial temperature profile.

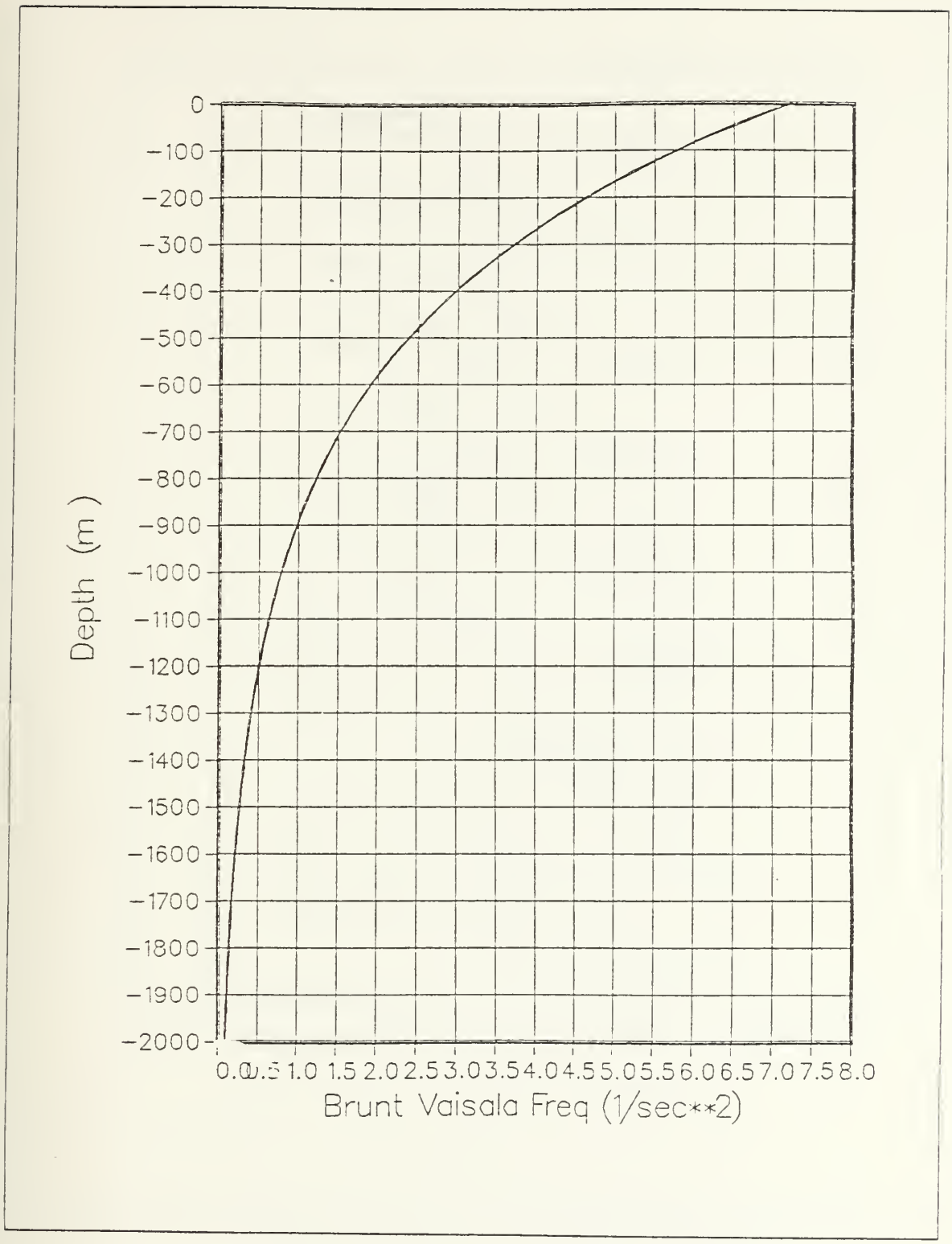

Figure 3.2 Initial profile of square Brunt-Vaisala frequency, N^2.

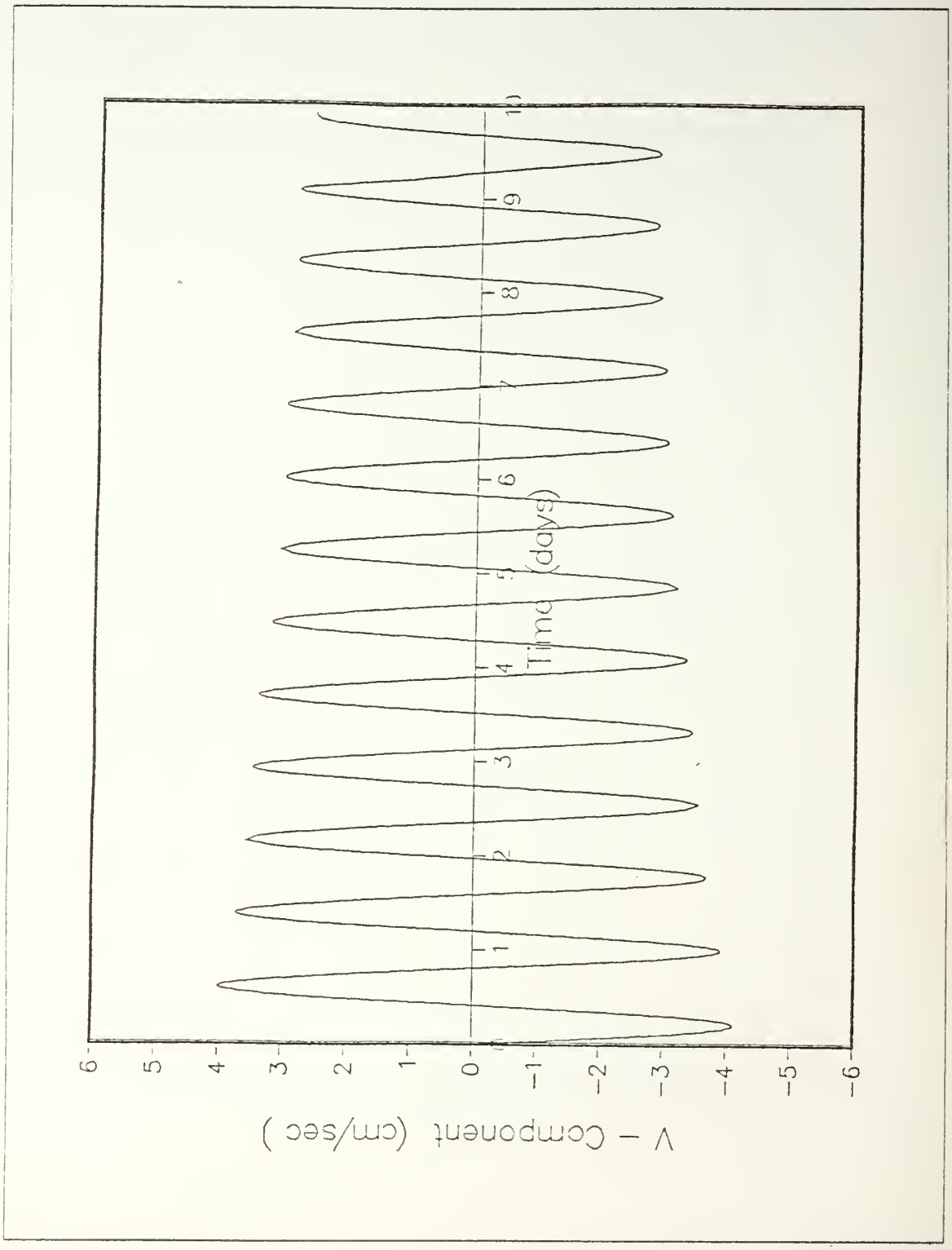

Figure 3.3 V-component inertial oscillations.

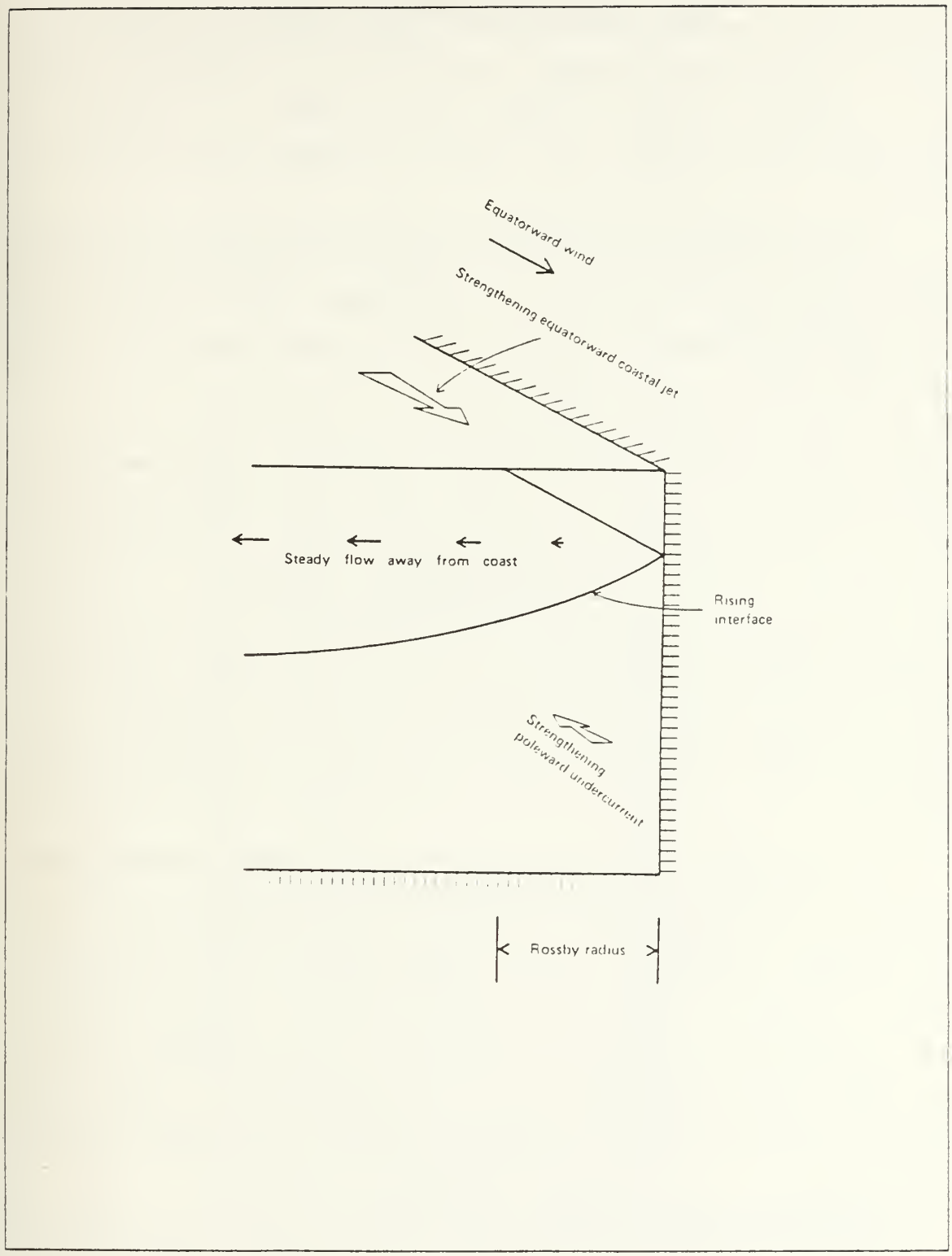

Figure 3.4 Schematic of coastal jet formation (from Gill, 1982).

gradient at day 30 (Figure 3.5) is 0.055°/km corresponding to a maximum surface, southward alongshore velocity component of 60 cm sec. At day 60 (Figure 3.6), the gradient of temperature has increased to 0.063° km with an associated maximum southward velocity of 80 cm sec. Finally, at day 90 (Figure 3.7), the gradient of temperature has further increased to 0.070° km with a maximum southward velocity of 100 cm sec.

The vertical structure of the developed jet is best described by computing the alongshore and ten-day time-average of the v-component of velocity and plotting that field as a function of cross-shore direction and depth. Figure 3.8 shows some interesting features. The depth of penetration of the southward flowing, coastal jet is approximately 1000 m with an offshore extent of approximately 100 km. The maximum surface velocity lies approximately 25 km offshore and the jet axis is vertically oriented with depth. The first internal Rossby radius of deformation was calculated to be 29.3 km, by the method of Feliks (1985), which coincides well with the position of the surface maximum, alongshore velocity component in this experiment. An undercurrent is present which is characterized as a deep, slow ($\sim$ 5 cm sec), poleward-flowing current underlying the southward flowing jet. This undercurrent has a maximum alongshore velocity component at the coast. Additionally, note that the weakest vertical shear occurs on the anticyclonic side (offshore or right side) of the southward-flowing jet. While it may not be easy to see from the figure, the largest magnitude of relative vorticity also occurs on the anticyclonic side of the jet in this experiment.

A cross-section of the alongshoreand time-averaged temperature field is shown in Figure 3.9. Away from the coast, the initial temperature stratification of 15° C at the surface and 2° C at depth, has only been slightly modified, if at all. However, the coastal stratification demonstrates a classical upwelling regime by the upward bending isotherms. As previously described, the horizontal temperature gradients established support the geostrophic jet (Figure 3.8). The surface, coastal temperature has been cooled, from an initial temperature of 15° C, to approximately 9° C. This coastal temperature structure has important implications in potential vorticity analysis and will be discussed later.

2. Experiment 2 (Wind with Curl)

Experiment 2 differed from experiment 1 only in that the forcing function included the important effect of wind stress curl. Idealized wind data (Figure 2.9)

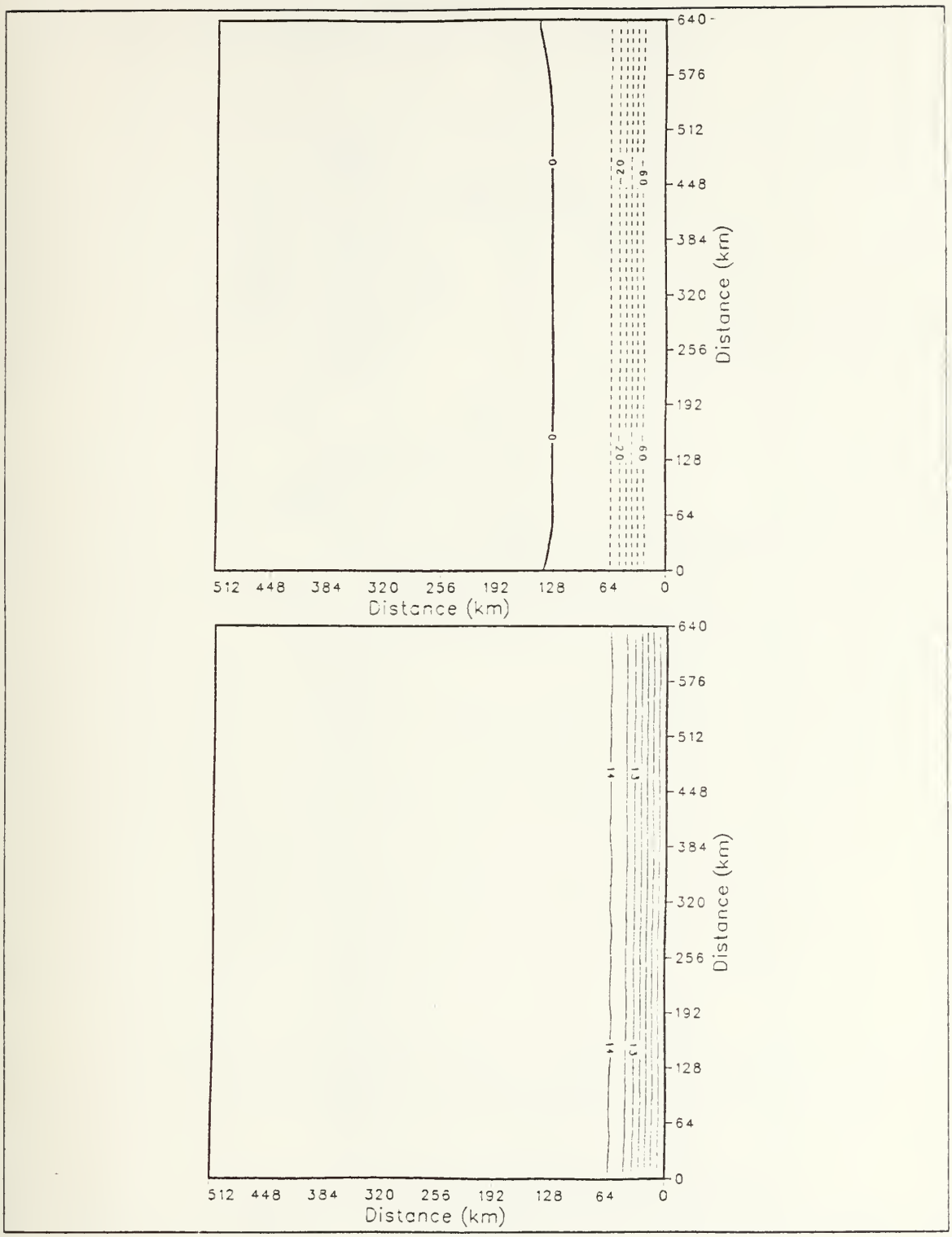

Figure 3.5 Contours of v-component velocity (top), cm/s and temperature (bottom), °C at day 30 for exp. 1.

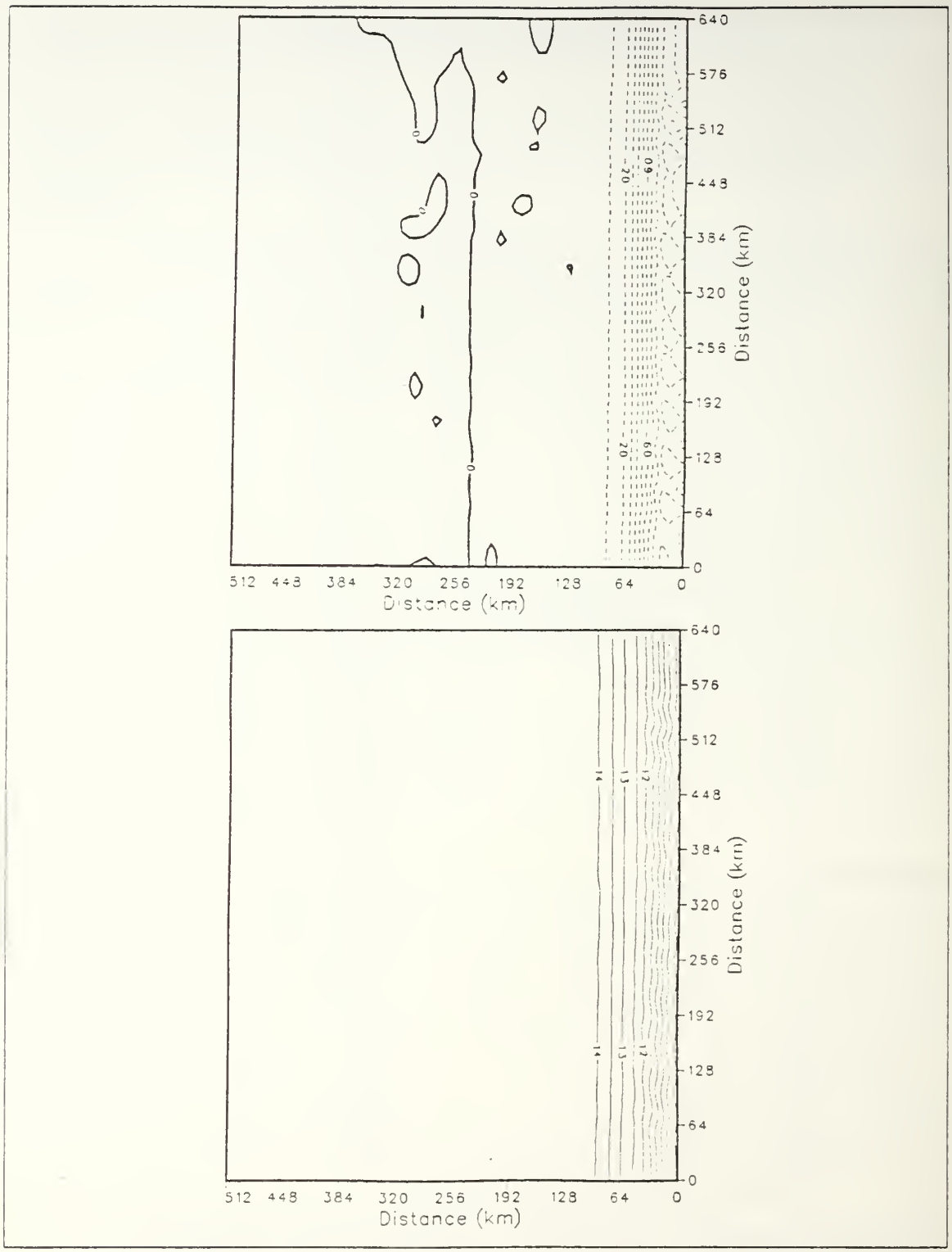

Figure 3.6 Same as Figure 3.5 except day 60.

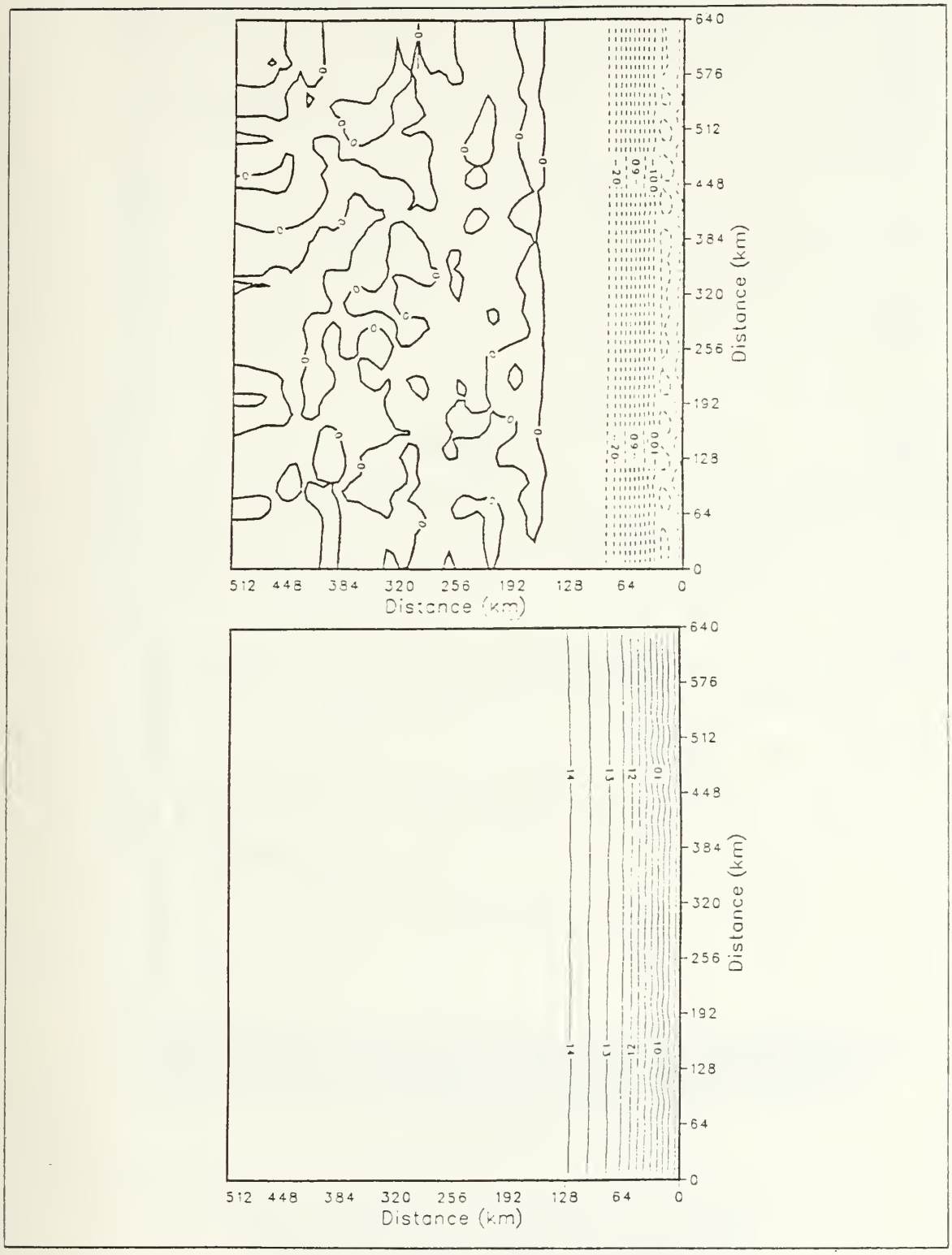

Figure 3.7 Same as Figure 3.5 except day 90.

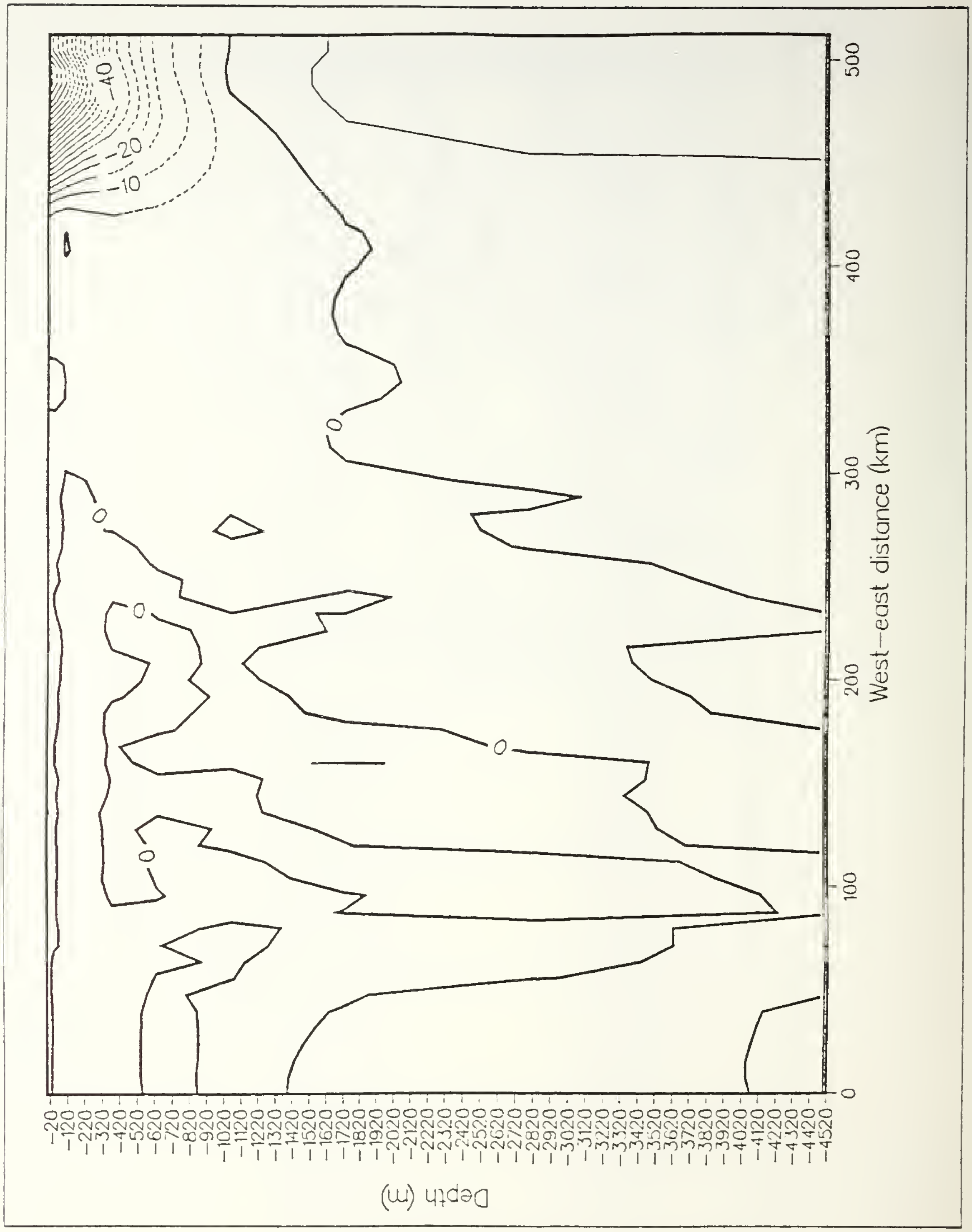

Figure 3.8 Cross-section of v-component velocity alongshore- and time averaged (days 81-90) experiment 1 - contour interval = 5 cm sec.

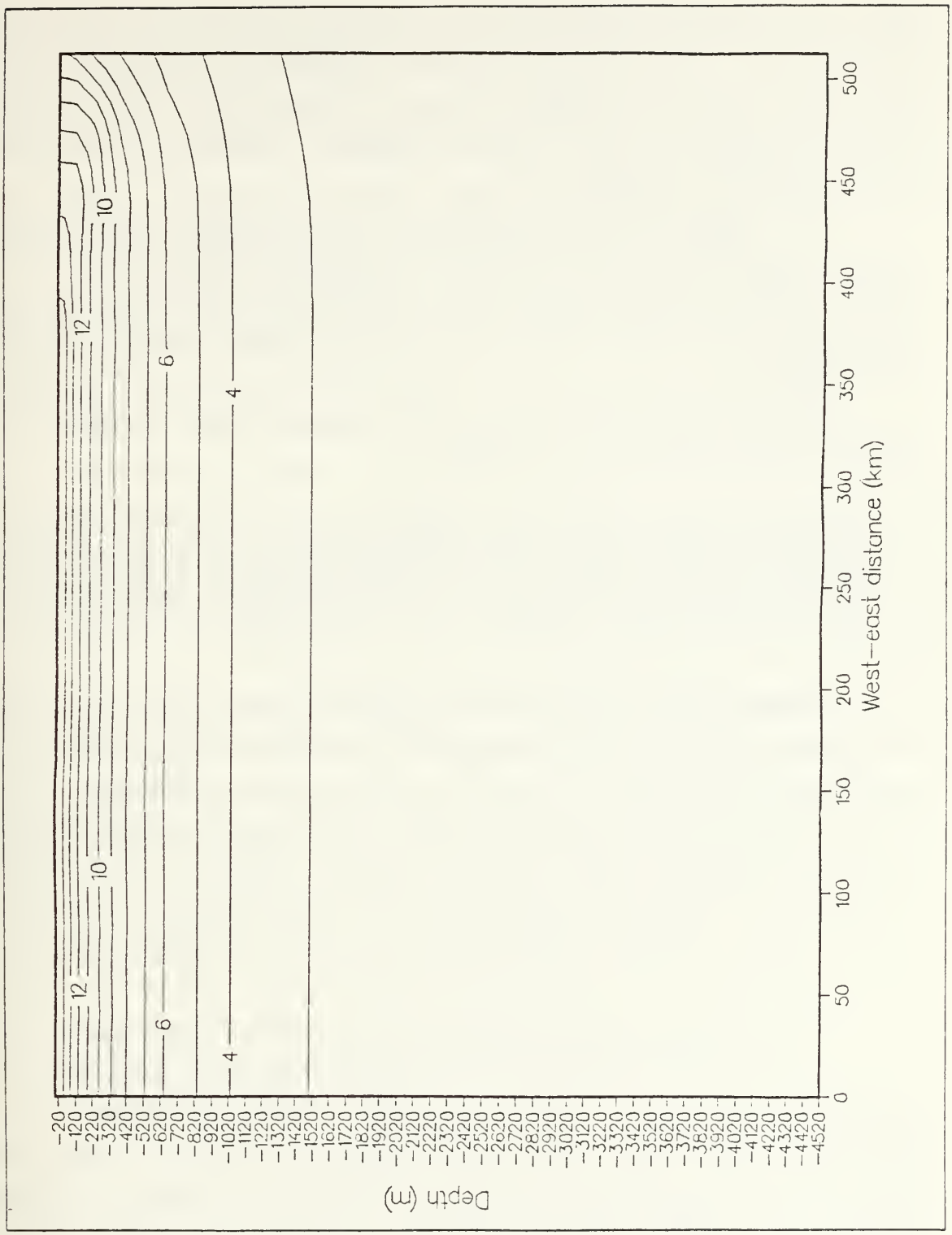

Figure 3.9 Same as Figure 3.8 except temperature contour interval = 1° C.

derived from the Gaussian representation of wind stress curl (eqn. 2.7), as described in Chapter II, was used to force the PE model in experiment 2. The inclusion of wind stress curl advanced the complexity, and realism, of model forcing because the wind was no longer uniform, as was the case in experiment 1. Otherwise, all aspects of the first two experiments were identical.

The idealized wind stress curl (Figure 2.7) has a maximum value at the coast of 0.65 dynes/cm^2/100 km which decreases to 0.00 dynes/cm^2/100 km at a distance of 187 km offshore. After the zero crossing, the wind stress curl continues to slowly decrease to a value of -0.11 dynes/cm^2/100 km at the western boundary of the PE model domain.

Nelson (1977) described the observed, long-term, mean climatological wind stress curl off the California coast as follows:

> Existence of an offshore wind stress maximum results in a line of zero wind stress curl approximately parallel to the coast. Positive curl occurs inshore of the maximum wind stress. Negative curl in the offshore region is associated with the anticyclonic atmospheric circulation over the interior ocean. The positive curl near the coast is related to topography and to local features in the surface wind stress distributions.

The main effect caused by wind stress curl is that the variation of wind stress in the offshore direction causes a variation in the Ekman transport which leads to convergence and divergence of mass. With the northerly wind blowing along the eastern boundary of the model, the positive curl produces oceanic, upper-level, horizontal divergence so fluid from below must be "sucked" vertically into the boundary layer to replace fluid transported away by mass divergence. The effect is Ekman pumping. Negative curl, conversely, creates mass convergence and causes downwelling (Figure 3.10). As previously discussed, the wind stress curl goes through zero at 187 km offshore and, therefore, the positive wind stress curl along the coast, causing Ekman pumping, will have a modifying effect on the coastal upwelling process described in section III.A.1. The effect of an offshore varying wind stress curl, as in experiment 2, is depicted by contours of the u-component of velocity during the initial model spin-up phase. Figure 3.11 clearly demonstrates that Ekman transport is a function of the strength of the northerly winds. Referring back to Figure 2.9, it is noted that the wind increases offshore to approximately 190 km and Figure 3.11 displays the corresponding increase in magnitude of the u-component to approximately

190 km. The u-component is negative (offshore) everywhere within the domain which is also consistent with Ekman transport being directed to the right of the wind. This offshore increase in the magnitude of the u-component of velocity is a representation of mass divergence resulting in Ekman pumping. Accordingly, proceeding past the zero crossing of wind stress curl further offshore, the magnitude of the u-component contours begins to decrease which is an indication of mass convergence.

A cross-section of the alongshore- and time-averaged v-component of velocity from experiment 2 is displayed in Figure 3.12. Striking differences in the structure and magnitude of the jet are immediately discernible in this figure when compared with a similar plot from experiment 1 (Figure 3.8). The offshore extent of the surface coastal jet in experiment 2 has increased by almost 90 km as compared with experiment 1. Note, however, that the effect is very shallow and quite weak. Albeit its relatively weak effect, the vertical shear on the offshore (anticyclonic) side of the coastal jet is, indeed, strengthened over that in experiment 1. The most noticable difference between the two profiles is the difference in the strengths of the jet. Figure 3.8 shows the maximum surface velocity of the jet to be -105 cm/sec whereas Figure 3.12 shows the maximum to be only -75 cm/sec. The explanation of this lies with the value of the wind at the coast in each experiment. Experiment 1 used a constant value of approximately -850 cm/sec (domain climatological value) whereas the coastal value of wind in experiment 2 was only about -630 cm/sec (coastal climatological average value). Coastal upwelling induced by the wind stress near the coast is clearly the dominant factor over Ekman pumping. A difference of only 2 m/sec ($\sim$ 5 kts) average wind speed can obviously produce a dramatic change in the oceanic response adjacent to the coast of California when the wind is northerly.

B. EXPERIMENTS WITH ZERO SLIP BOUNDARY CONDITIONS

1. Experiment 3 (Uniform Wind)

The zero-slip boundary condition at the eastern boundary was introduced into experiments 3 and 4. The importance of the free-slip versus the zero-slip boundary condition was addressed in Chapter II and it has been the subject of study by ocean circulation modelers since the studies of Bryan (1963) and Veronis (1966). Blandford (1971) demonstrated that the large difference between solutions obtained by Veronis and Bryan was caused by the difference between the free-slip and zero-slip conditions

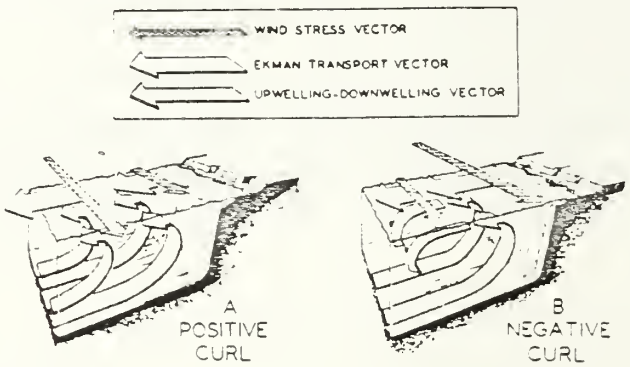

Figure 3.10 Schematic of Ekman pumping (from Gill, 1977).

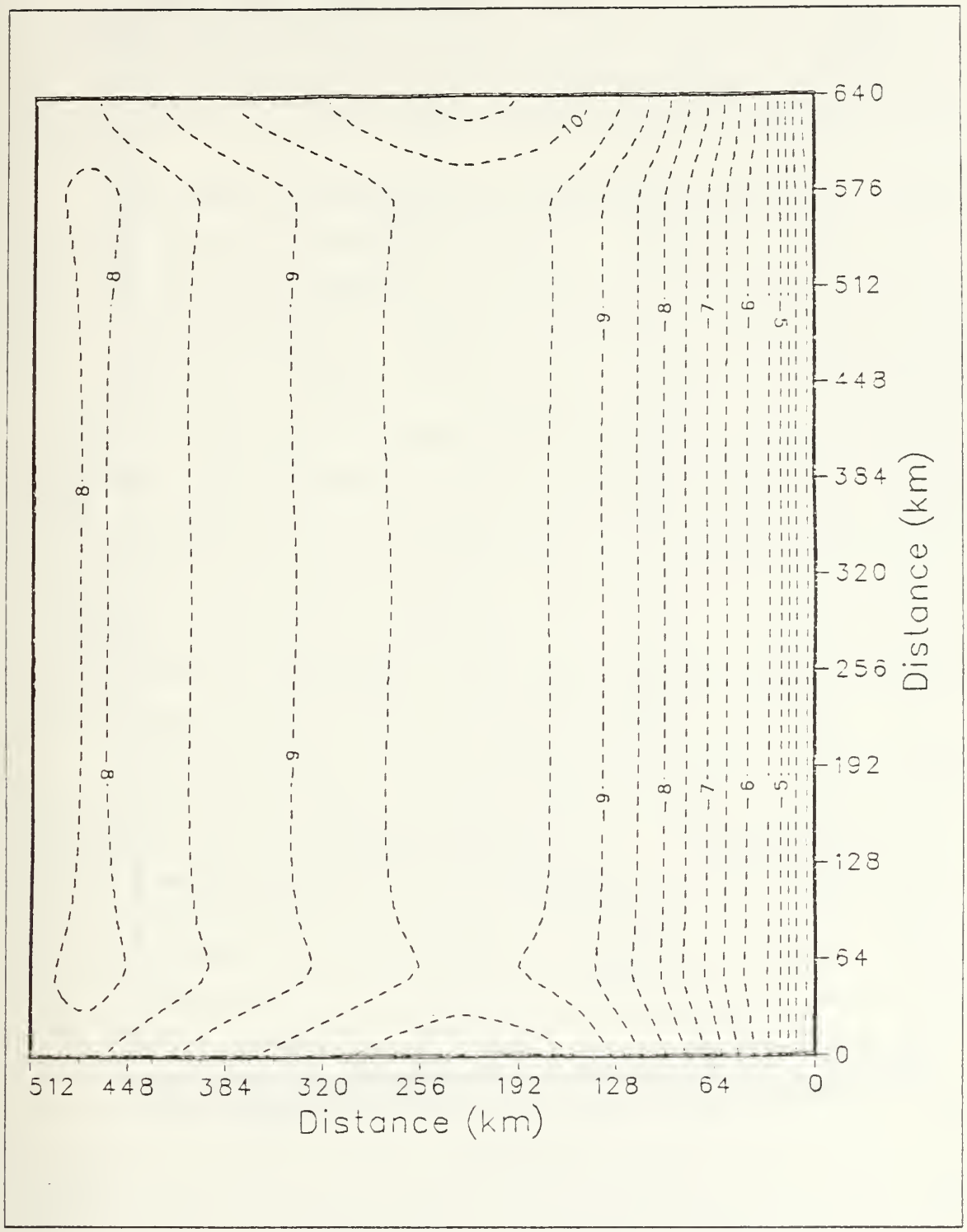

Figure 3.11 Contours of u-component velocity
contour interval = 0.5 cm sec
experiment 2 - day 6.

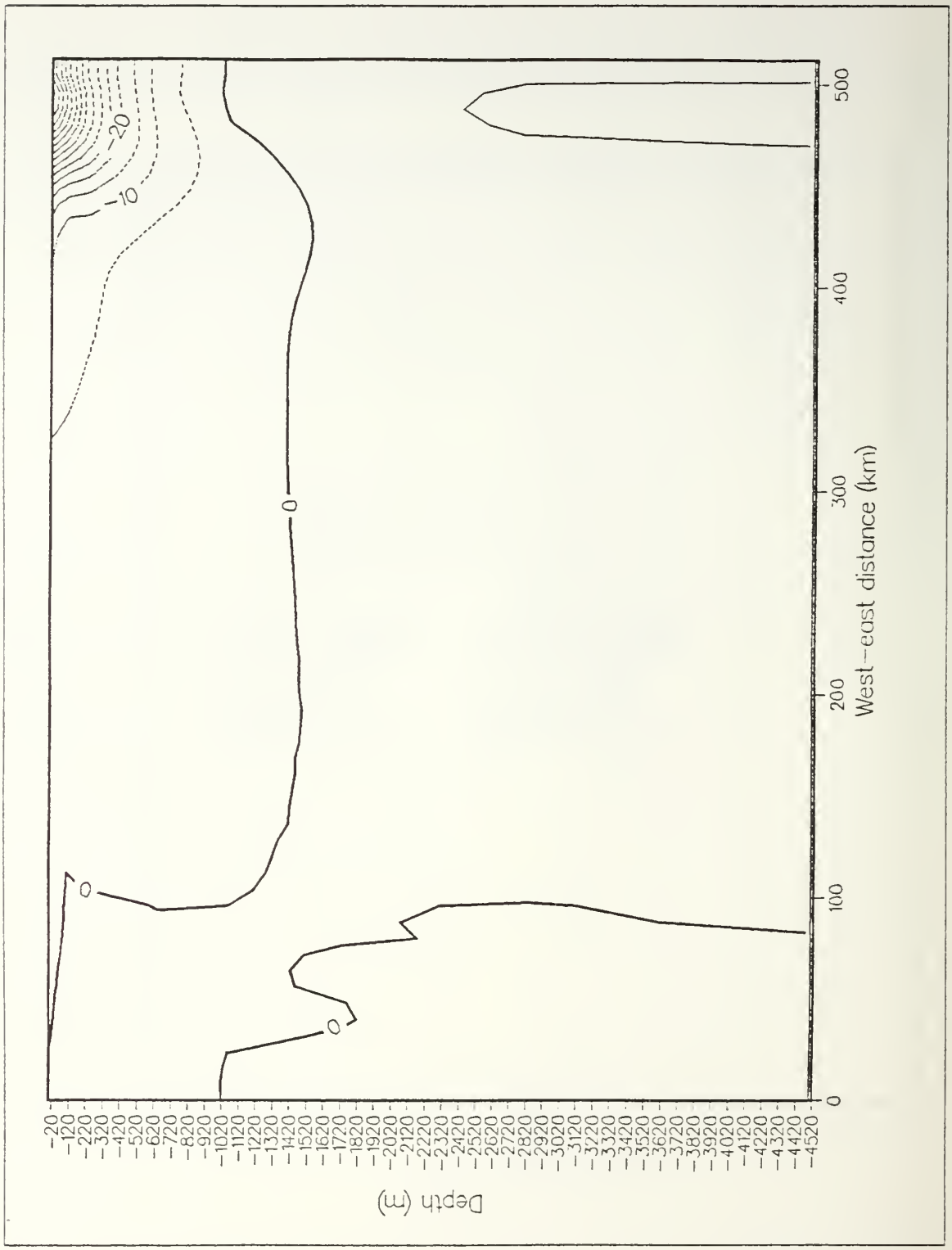

Figure 3.12 As in Figure 3.8 except experiment 2.

used. Veronis' free-slip condition produced a maximum velocity at the coast while the zero-slip condition used by Bryan produced a maximum velocity offshore. It is known that barotropic instability can occur if the profile curvature changes sign (Haltiner and Williams, 1980) and the zero-slip solution of Bryan's certainly satisfied that necessary condition.

Experiment 3, as stated previously, included the zero-slip boundary condition. All other aspects of the model were identical to experiment 1. Figure 3.13 is a normalized plot of the alongshore (v) component of velocity averaged in time (days 86-90), in depth (surface to ~ 1000 m), and alongshore. For comparison, a similar plot is displayed for experiment 1 (Figure 3.14). The effects of the zero-slip boundary condition employed in experiment 3 are immediately apparent. The frictional influence of zero-slip on the near-shore tangential velocity (v-component) dramatically reduced the coastal velocity as compared to the coastal velocity generated in experiment 1 with the free-slip condition. Therefore, the main effect of the zero-slip boundary condition is to significantly increase the cyclonic horizontal shear on the inshore side of the jet. The cyclonic horizontal shear in experiment 1 was $.15 \times 10^{-1}$ s^{-1} whereas the zero-slip condition increased the shear in experiment 3 to $.6 \times 10^{-1}$ s^{-1}. Another effect of the zero-slip condition in experiment 3 was to move the depth-averaged coastal jet axis approximately 8 km farther offshore than that in experiment 1 (free-slip).

As discussed earlier, a major result of Bryan's zero-slip boundary condition study was that the maximum alongshore velocity was located offshore causing the necessary condition of barotropic instability (profile curvature changes sign) to be satisfied, whereas the free-slip study by Veronis did not satisfy that necessary condition. In this study, the zero-slip condition was not an essential requirement to satisfy the necessary condition of barotropic instability. It can be seen that experiment 1, which had the free-slip condition, also satisfied the necessary condition (evident by the jet profile curvature changing sign approximately 75 km offshore in Figure 3.14). The upwellinginduced coastal jet, simulated in this eastern boundary study, has a velocity maximum offshore regardless of the boundary condition used (free-slip or zero-slip). In contrast, the western boundary current in the free-slip study by Veronis had a maximum velocity at the coast which prevented the profile curvature from changing signs. Apparently, the baroclinicity of the modeled upwelling-induced coastal jet dominates the positioning of the jet axis over the effects of the frictional eastern boundary condition.

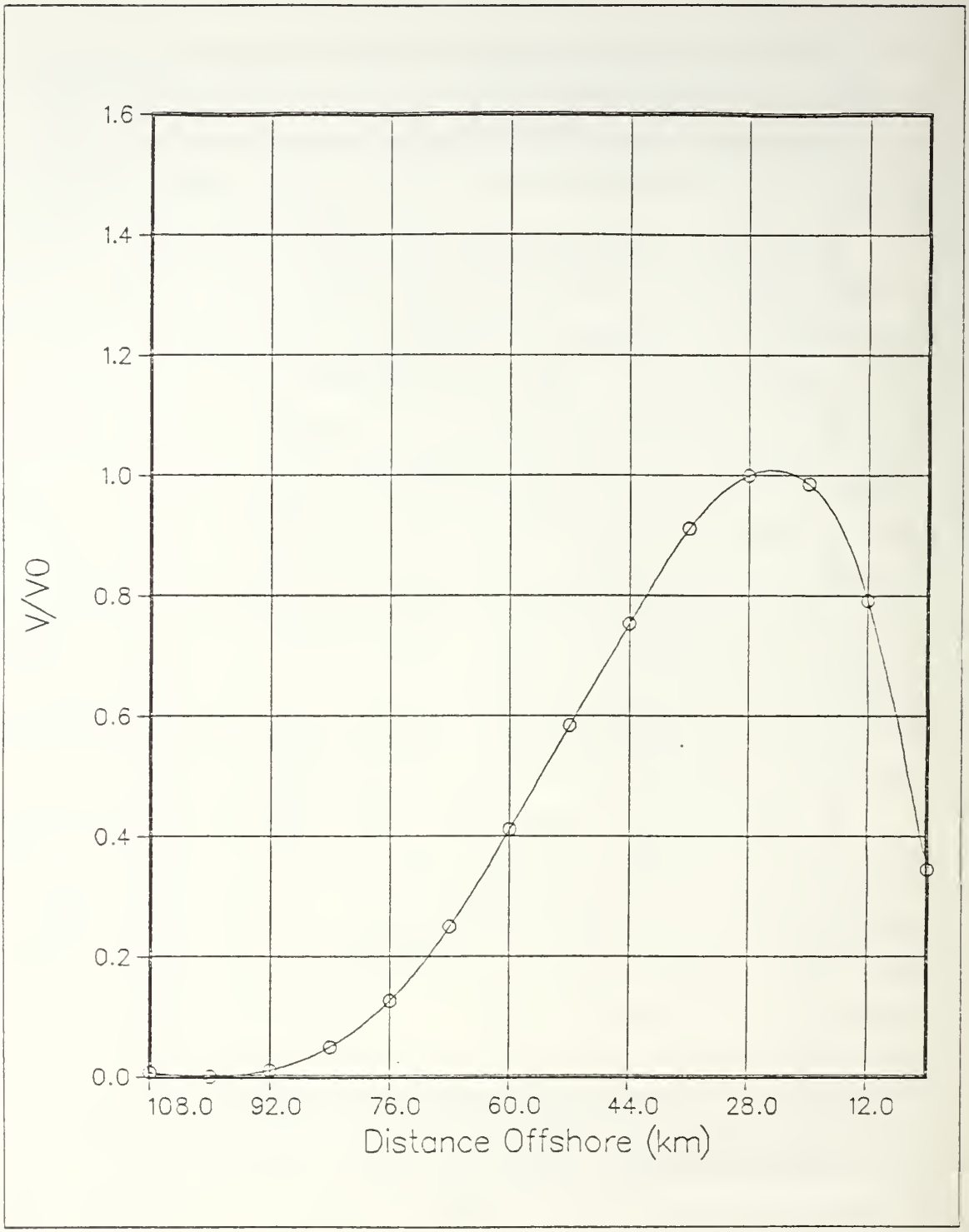

Figure 3.13 Normalized alongshore velocity averaged in time, depth, and alongshore experiment 3.

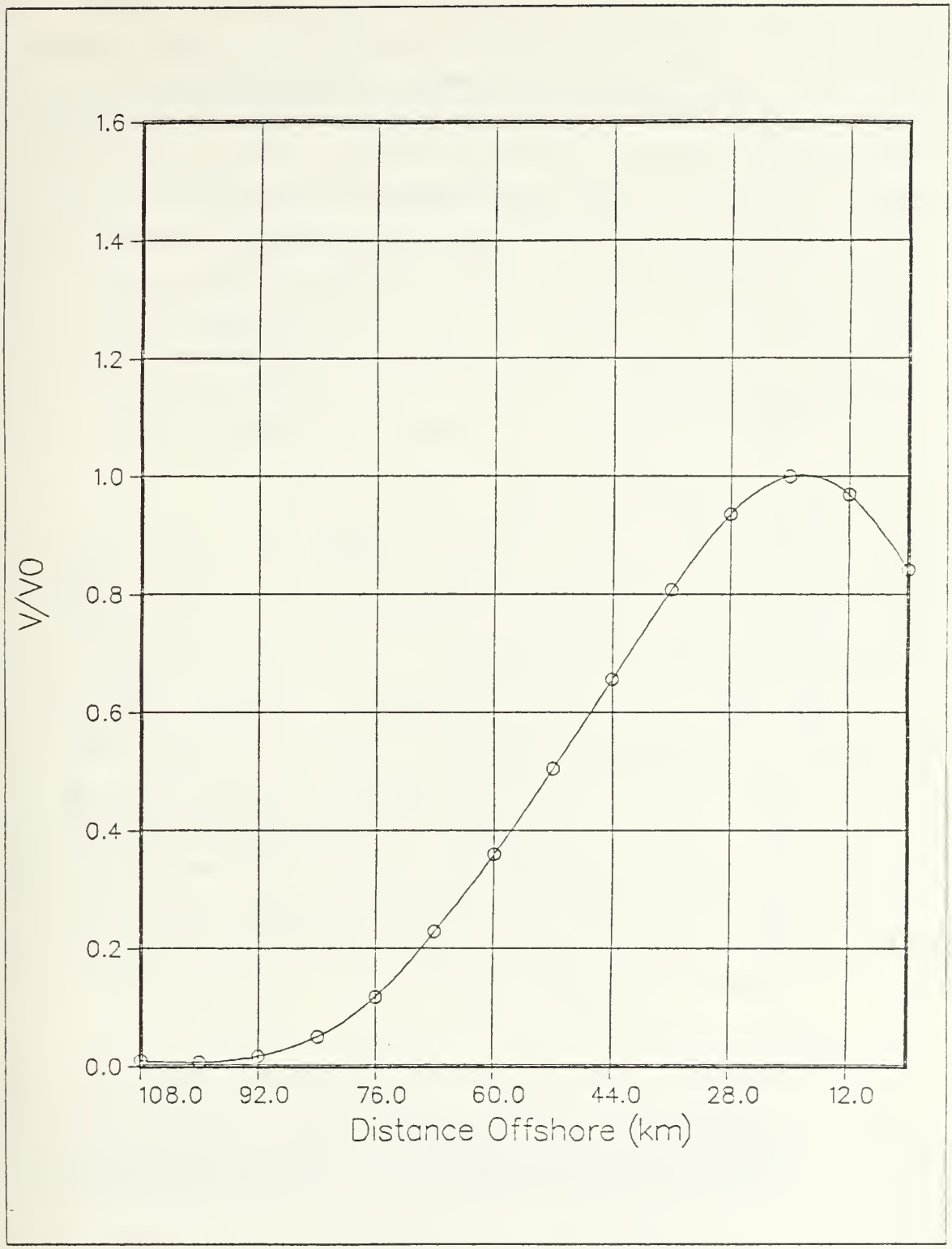

Figure 3.14 Same as Figure 3.13 except experiment 1.

It is again interesting to analyze the timeand alongshore-averaged cross-section of the v-component of velocity. Figure 3.15 is the profile generated by experiment 3. The effect of a zero-slip boundary condition is immediately apparent in this plot. The tangential velocities along the coast in experiment 3 are much less than those generated in experiment 1 (Figure 3.8). Because of this, the coastal isotachs, in experiment 3 are sloped upward which significantly reduces the vertical shear on the inshore (cyclonic) side of the jet as compared with experiment 1. The result is that the jet is more symmetric in the offshore direction. However, the positive vorticity on the inshore side of the jet is now about twice as big as the negative vorticity on the offshore side. This is very different from the pattern in experiment 1 (Figure 3.8). Another interesting result of the zero-slip boundary condition is that the northward flowing undercurrent maximum has also moved further offshore along with the coastal jet.

2. Experiment 4 (Wind with Curl)

As an extension of the zero-slip boundary condition study, experiment 4 incorporated zero-slip on the eastern boundary along with the wind stress curl as in experiment 2. Except for the zero-slip condition, all other aspects of the model in experiment 4 were identical to experiment 2. As would be expected, the basic characteristics of the zero-slip boundary condition, as described in the results of experiment 3, were reproduced in experiment 4. Again, the vertical shear on the cyclonic side of the jet was decreased by the upward-bending isotachs near the coast. As in experiment 3, this increased the horizontal shear, and hence the relative vorticity on the inshore side of the jet. The undercurrent maximum is the narrowest of all four experiments and its alongshore velocity maximum lies furthest offshore due to the combined effects of wind stress curl and zero-slip. Figure 3.16 demonstrates the salient features of the mean velocity profile.

C. STABILITY ANALYSIS

It is now well known that, at times, the instantaneous California Current consists of "intense meandering current filaments (jets) intermingled with synoptic-mesoscale eddies" (Mooers and Robinson, 1984). The exact generation mechanism, or source, of the observed eddies and their role in the dynamics of the CCS have yet to be determined. One hypothesis currently under investigation is that the eddies are locally generated through dynamic instability of the seasonal mean flow. Thomson (1984)

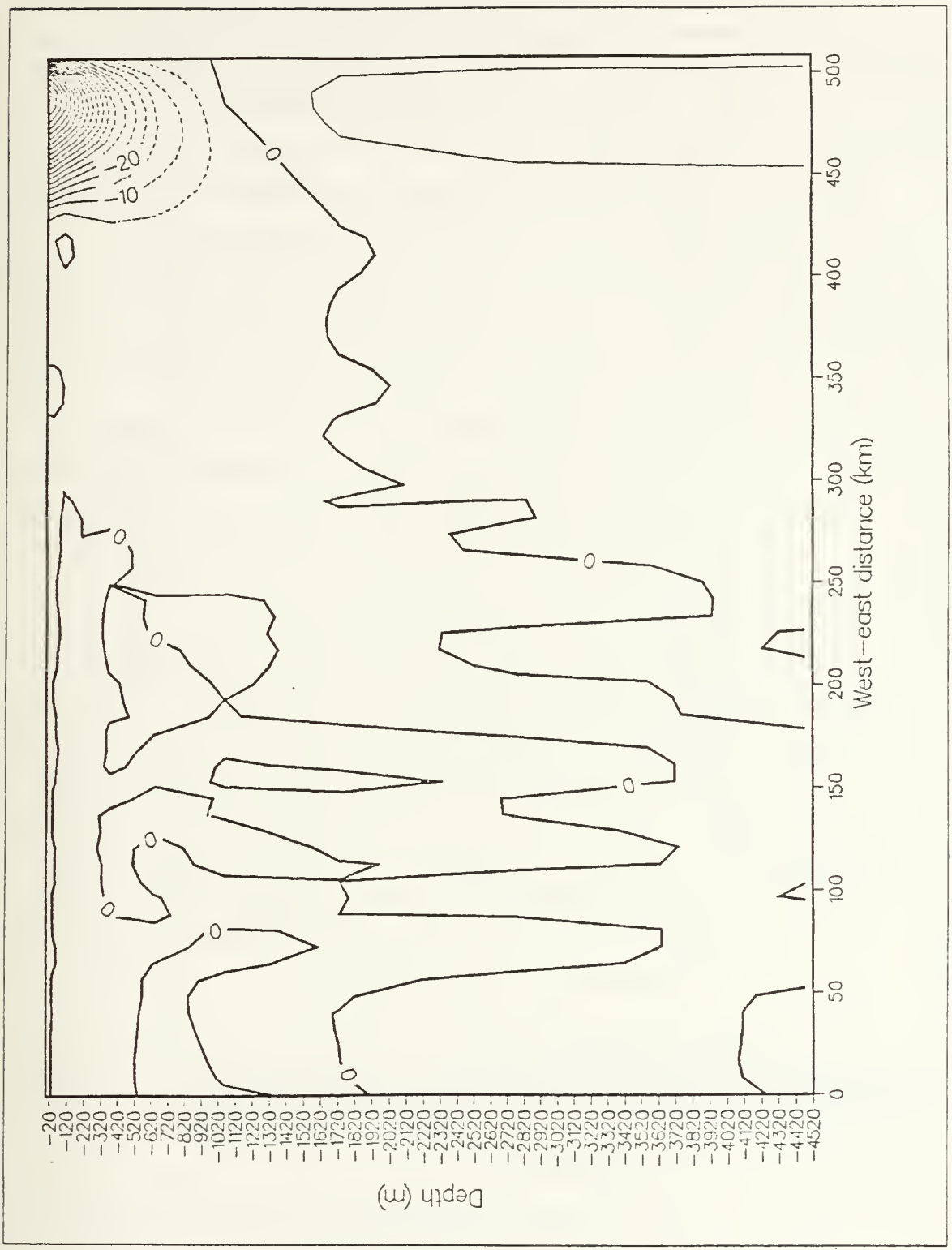

Figure 3.15 Same as Figure 3.8 except experiment 3.

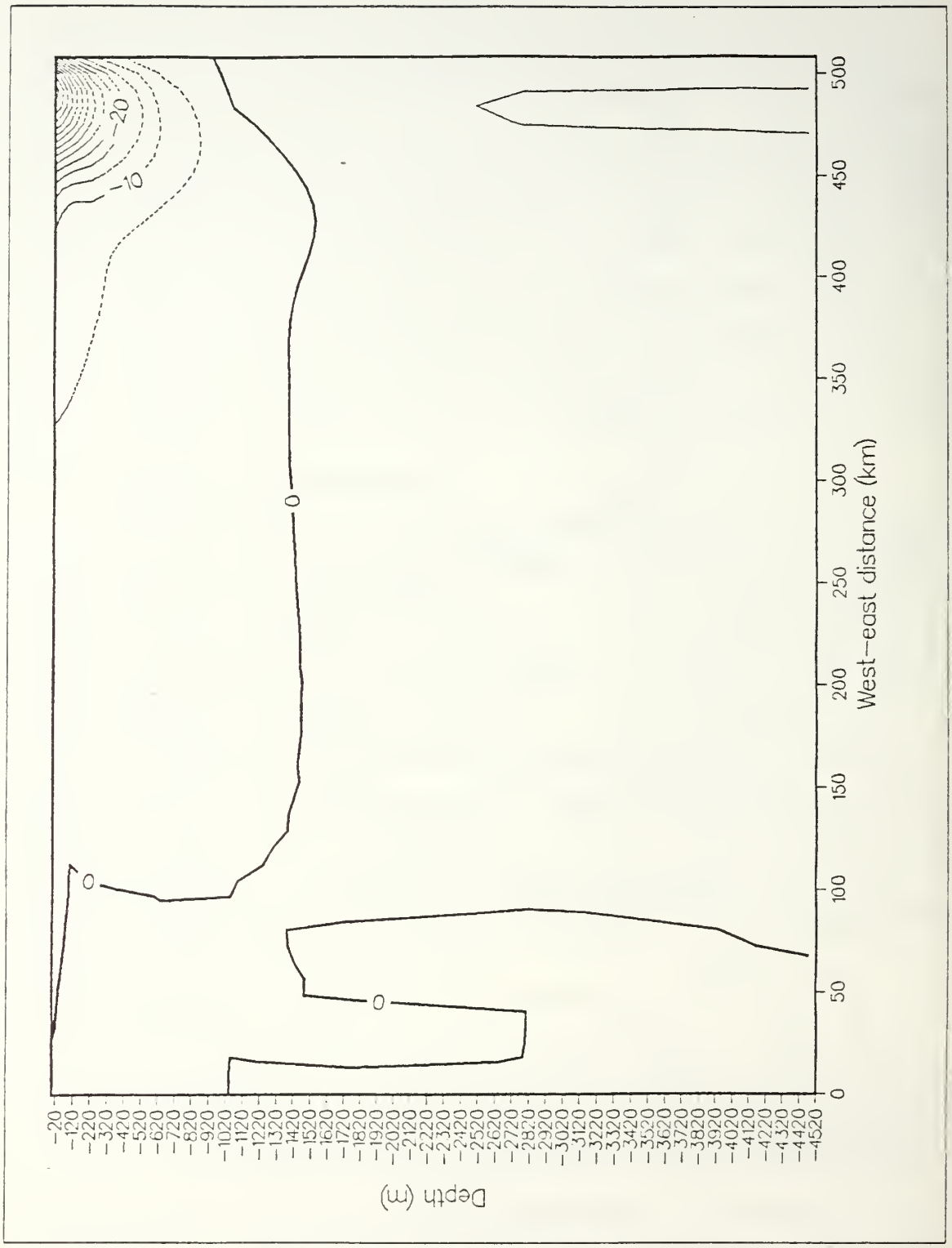

Figure 3.16 Same as Figure 3.8 except experiment 4.

presented a strong case of an observed cyclonic eddy which formed over the continental margin of Vancouver Island through the process of baroclinic instability with an additional, yet secondary, contribution from barotropic instability. He furthermore suggested that the energy for the instability was derived from the vertical shear of the geostrophic flow associated with a southeastward surface current and a northwestward subsurface flow representative of the California Undercurrent.

In the previous sections of this chapter, the coastal jet profile was described for each experiment and was shown to satisfy the necessary condition for barotropic instability. The results of Thomson (1984) suggest that a more important source may be baroclinic instability of the mean flow. Of the four experiments discussed in this chapter, none developed instability and, therefore, eddies and current filaments were not generated. However, it is extremely important to analyze the mean flow to establish its potential for mixed (barotropic and baroclinic) instability. If potential for instability indeed exists in the mean flow generated by the PE model, it may provide insight into the complexities of eddy generation in the CCS.

Implications of the distribution of potential vorticity as a signature of instability have been examined by Watts and others (Robinson, 1983) for the Gulf Stream. Watts stated that potential vorticity, used as a conservative quantity, can serve as a tracer in the ocean. Additionally, the cross-stream distribution of potential vorticity may be used as a test of predictions by quasigeostrophic theory regarding necessary conditions for unstable growth of fluctuations. The conditions which are necessary for instability to occur are very useful because, if they are not satisfied, it can be concluded that the dynamical constraints will not allow available energy to be released (Gill, 1982). One of the conditions is that the cross-stream derivative of potential vorticity must change sign somewhere within the domain. Another condition is that the product of the cross-stream derivative with the basic current must be positive. Also, theory formally requires a basic state current which is slowly changing in space and time, so that linearization applies for perturbation quantities (Robinson, 1983) ; this requirement is met by the structure of the coastal jets generated in this study.

The following expression, in cartesian coordinates, used by Watts to examine the potential vorticity (q) signature in the Gulf Stream, will by used to examine potential instability of the coastal jet generated in this study:

$$q \sim (f + \zeta) \frac{\partial T}{\partial z} - \frac{\partial T}{\partial x} \frac{\partial v}{\partial z} \quad , \tag{3.3}$$

where

$$\zeta = \frac{\partial v}{\partial x} - \frac{\partial u}{\partial y} \quad . \tag{3.4}$$

Figure 3.17 shows a cross-section of contours of the time-averaged (days 81-90) and meridionally-averaged potential vorticity for experiment 1 in units of °C m^{-1} sec^{-1} scaled by 10^6. Similarities in the structure of the potential vorticity field between the Gulf Stream (Figure 3.18) and the simulated California Current (Figure 3.17) are apparent. There is a tendency for potential vorticity to be uniform along isothermal surfaces and also to change vertically in the same manner as the offshore temperature stratification. The potential vorticity field for experiment 1 is further characterized by the following features:

- The range of potential vorticity lies between 0.0-2.5 × 10^{-6} °C m^{-1} sec^{-1}.
- A relative minimum exists in the surface layer caused by weak stratification due to turbulent vertical mixing.
- A stronger relative minimum exists in a thicker surface layer near-shore due to upwelling induced weak stratification.
- A relative maximum in potential vorticity exists in the middle to western part of the domain at a depth of ~ 90 m (the "seasonal" thermocline in the model).
- A change in the sign of the slope of potential vorticity contours is apparent in the east-west direction of the upper levels, near-shore.

One difference between the potential vorticity field in the Gulf Stream and that in the simulated CCS is the difference in magnitude of potential vorticity. The magnitude of potential vorticity in the Gulf Stream is approximately twice that in the simulated CCS. This difference is mainly attributable to the difference in temperature stratification between the Gulf Stream and the CCS. From the isotherms depicted in Figure 3.18 it can be seen that the strongest stratification in the Gulf Stream approaches ~ 10 ° C over 140 m or 0.07 °C/m, whereas from Figure 3.9 the maximum temperature stratification for experiment 1 is only ~ 3.5 °C over 140 m or 0.03 °C/m. Note that Figure 3.18 was constructed by the approximation of potential vorticity, $q \sim f\, \partial T/\partial z$, whereas Figure 3.17 was constructed from the full form of potential vorticity (eqn. 3.3). The neglected term in Watts' approximation was found to contribute between 10 and 20% of the potential vorticity in most cases and, in particular, the second term dominated in experiment 1 on the near-shore, cyclonic side

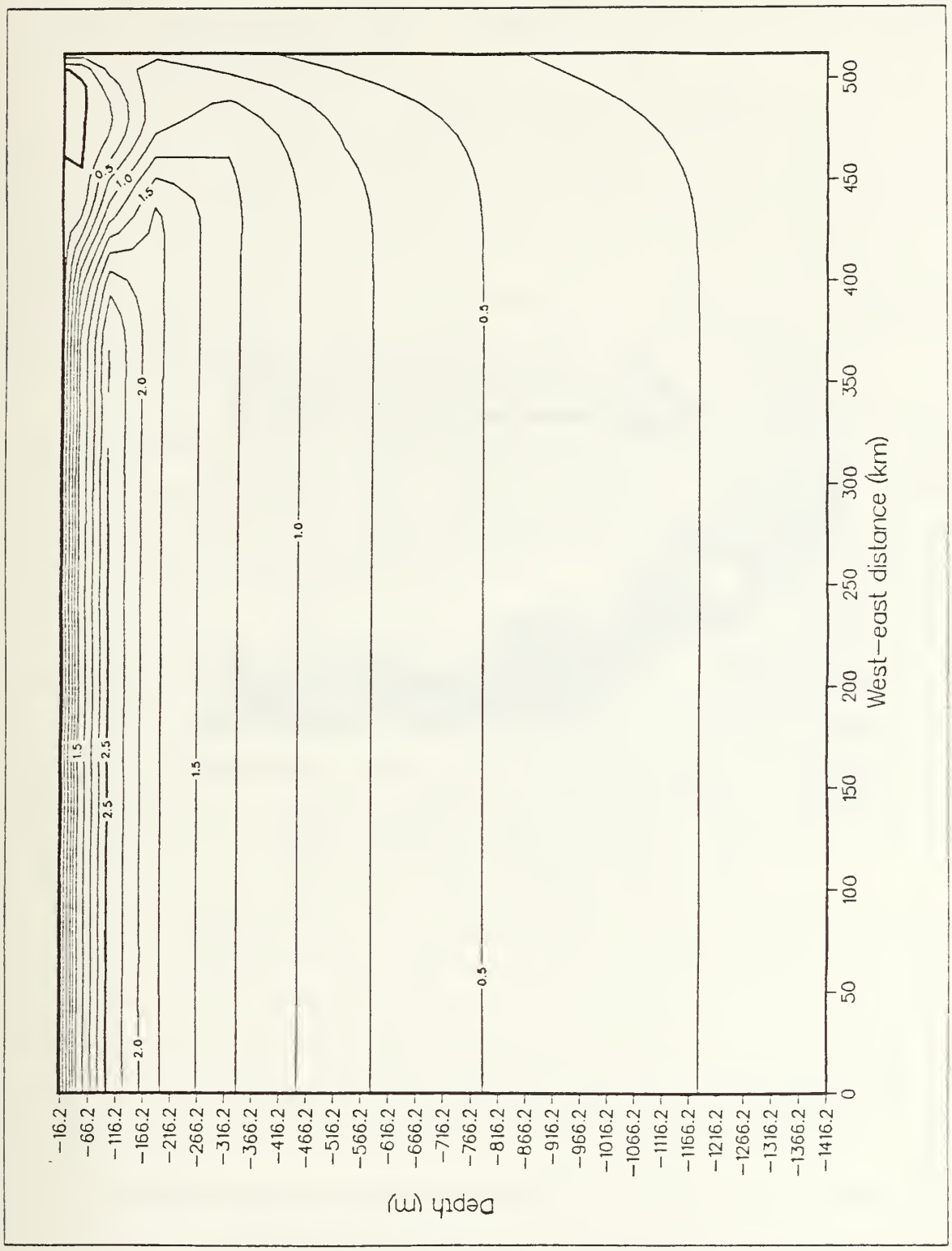

Figure 3.17 Potential vorticity in the CCS (exp. 1).

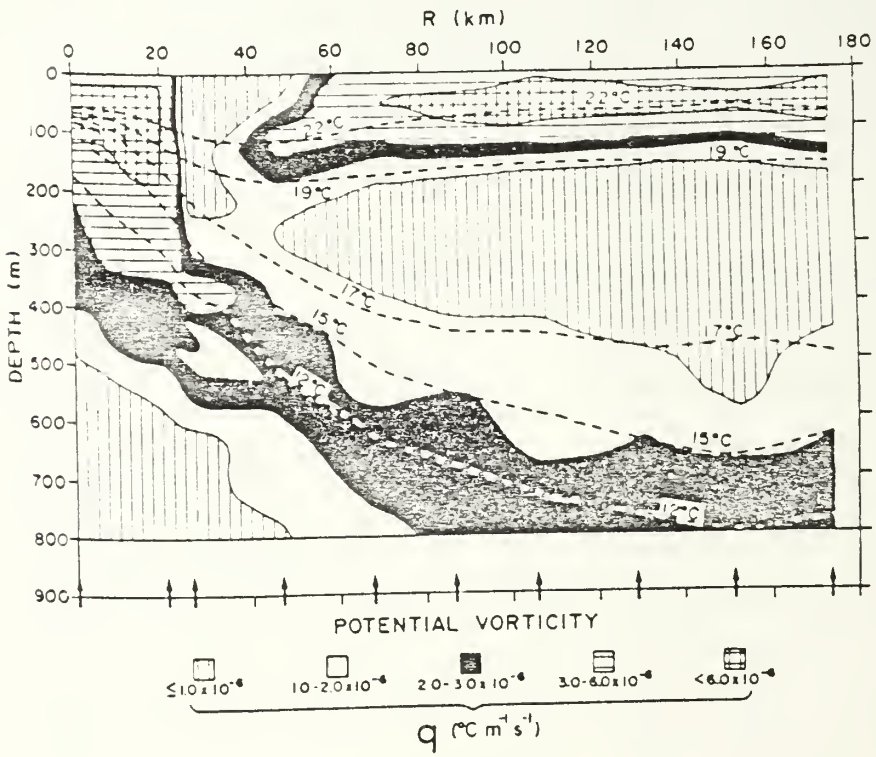

Figure 3.18 Same as Figure 3.17 except for the Gulf Stream (from Robinson, 1983).

of the coastal jet. The scaled form of potential vorticity was used in the Gulf Stream analysis due to limitations in data. As a result of this, only qualitative comparisons have been made between analyses.

As previously discussed, a necessary condition for instability is that the cross-stream derivative of potential vorticity must change sign somewhere within the domain. To examine the potential vorticity field for this condition, the horizontal gradient was computed ($\partial q / \partial x$) and multiplied by one grid length (ΔX) for scaling purposes. The resultant cross-stream derivative is displayed in Figure 3.19 for experiment 1. As expected from Figure 3.17, the cross-stream derivative changes sign in the upper levels across the extent of the simulated coastal jet. The necessary condition for instability of the mean flow was therefore, easily satisfied in experiment 1.

The other experiments conducted in this study displayed very similar patterns of the cross-stream gradient of potential vorticity and, therefore, all will not be shown. All of the experiments satisfied the necessary condition for instability. There was no significant difference in the gradient of potential vorticity between the experiments with uniform wind and those which included wind stress curl. However, the gradient of potential vorticity in the experiments with zero-slip was stronger (both positive and negative) than those with the free-slip boundary conditions because of the additional contribution from horizontal shear as discussed in section III.B.1. (see Figure 3.20).

Why, then, if the necessary condition for instability has been satisfied in each experiment, has the mean flow not gone unstable? The answer to that question is not readily apparent. It is useful, though, to explore a simple baroclinic instability model to determine what the sufficient conditions are for baroclinic instability of the mean flow.

The simplest model which can incorporate baroclinic processes is a two-layer model. Following the method of Holton (1979), the ocean is divided into two discrete layers. In all of the experiments conducted in this study, the southward-flowing coastal jet extended to approximately 1000 m in the vertical. For this reason, the upper model layer extends from the surface to 500 m depth and the lower layer extends from 500 to 1000 m. See Table 3 for the arrangement of variables in the vertical for the two-layer baroclinic model.

The QG vorticity equation is applied at levels 1 and 3 whereas the QG thermodynamic equation is applied at level 2. The streamfunction, ψ_2 is obtained by linearly interpolating between -250 m and -750 m. This forms a closed set of prediction equations with $\beta = 0$, as in the PE model.

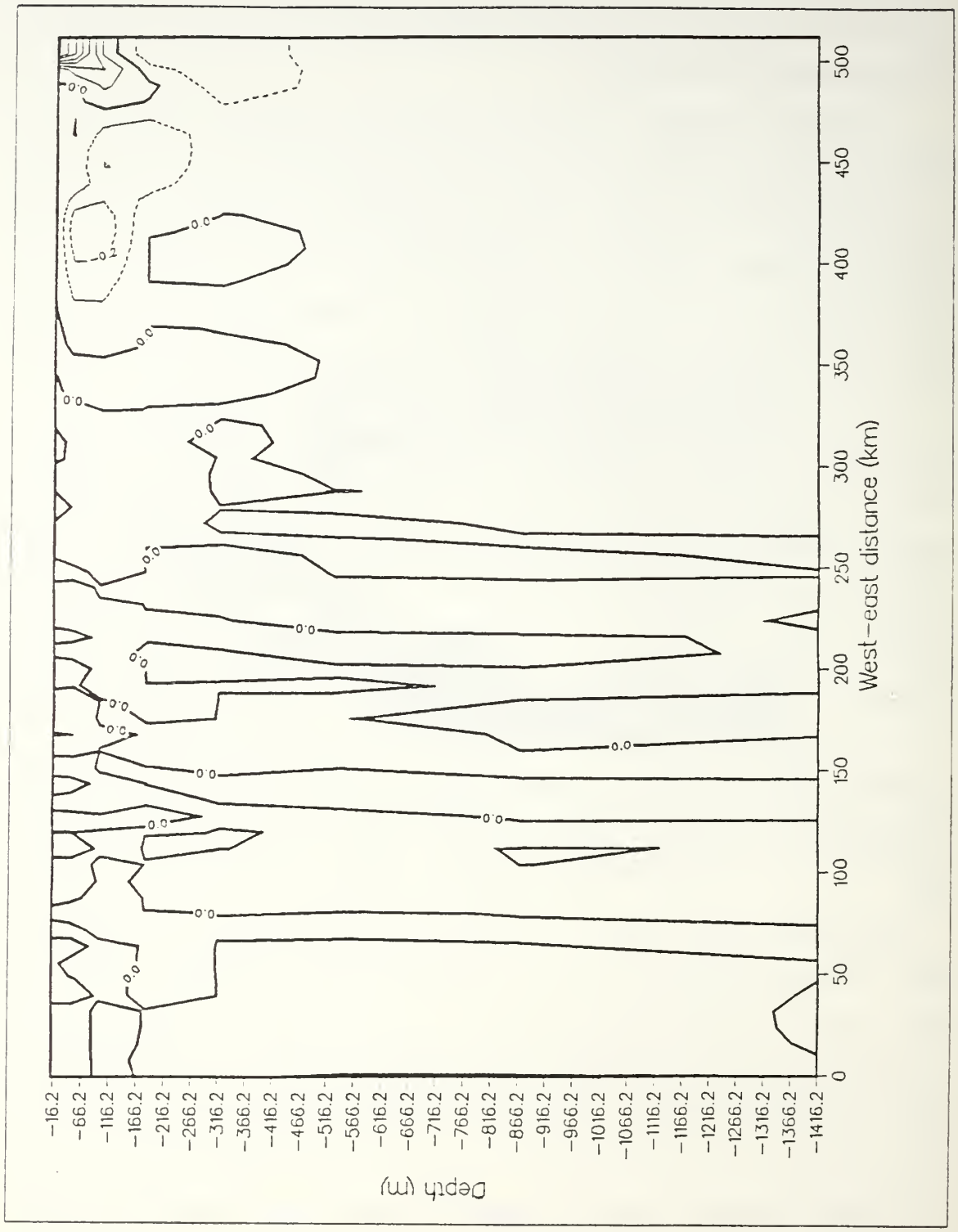

Figure 3.19 Cross-stream derivative of potential vorticity experiment 1.

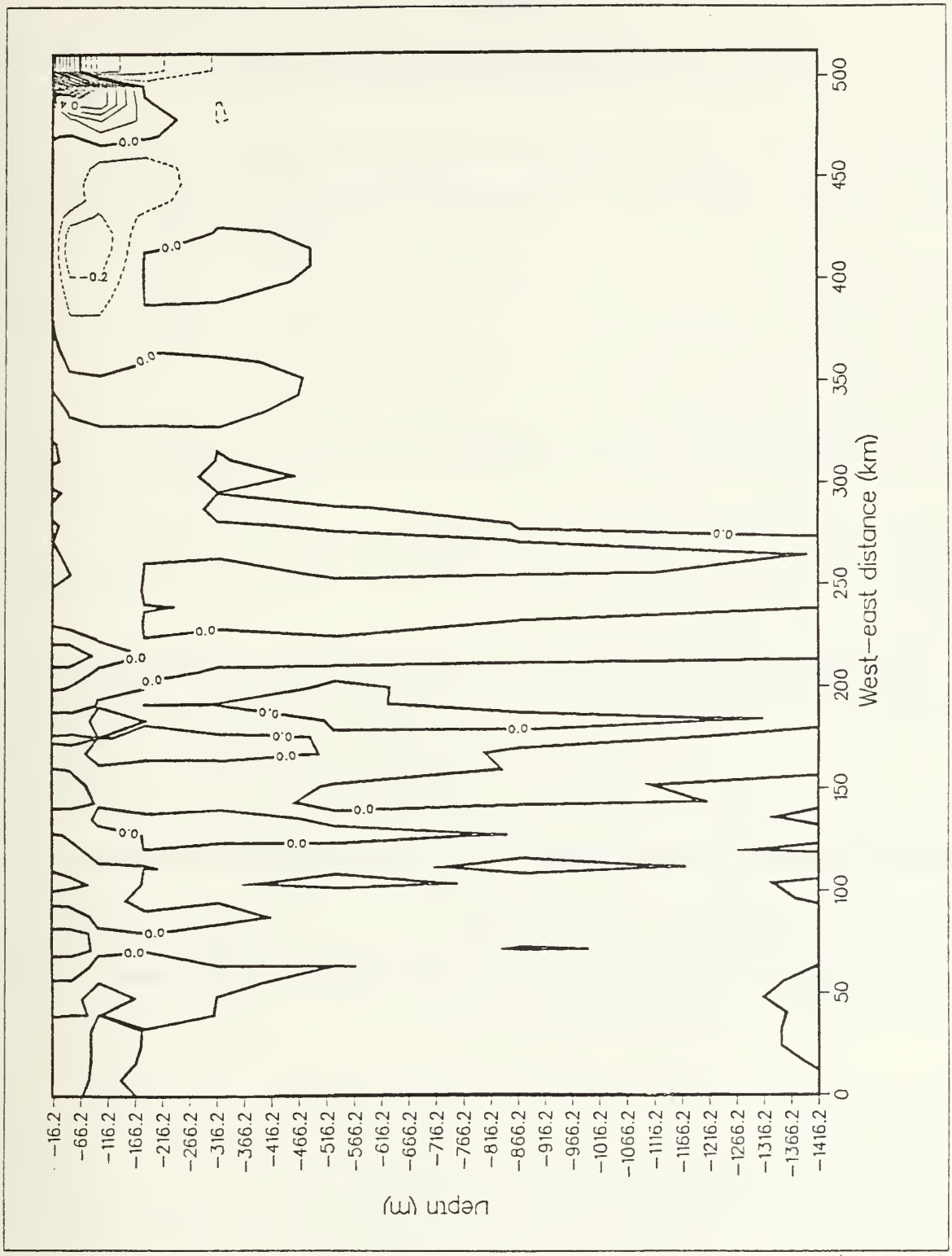

Figure 3.20 Same as Figure 3.19 except experiment 3.

TABLE 3

ARRANGEMENT OF VARIABLES IN THE VERTICAL FOR THE TWO-LAYER BAROCLINIC MODEL

0 m	————	$w_0 = 0$	————	level 0
-250 m	----------	ψ_1	----------	level 1
-500 m	————	w_2	————	level 2
-750 m	----------	ψ_3	----------	level 3
-1000 m	————	$w_4 = 0$	————	level 4

The length scale used in this model is the Rossby radius of deformation (λ^{-1}) defined by:

$$\lambda^2 \equiv \frac{f_0^2}{\sigma (\Delta z)^2} , \qquad (3.5)$$

where Δz is the layer thickness (500 m) and σ is the stability parameter defined by:

$$\sigma = \alpha g \partial T / \partial z . \qquad (3.6)$$

The phase speed (c) is obtained from solving the closed set of QG equations, by assuming wave-type solutions, yielding:

$$c = V_M \pm V_T \left[\frac{k^2 - 2\lambda^2}{k^2 + 2\lambda^2} \right]^{1/2} , \qquad (3.7)$$

where the vertically averaged current (V_M) is defined as:

$$V_M \equiv \frac{V_1 + V_3}{2} , \qquad (3.8)$$

and the basic state "thermal wind" (V_T) is defined as:

$$V_T \equiv \frac{V_1 - V_3}{2} \quad . \tag{3.9}$$

For waves with meridional wavenumbers (k) satisfying $k^2 < 2\lambda^2$, there exists an imaginary component of the phase speed (c_i). This criteria defines the critical wavelength (L_c) as follows:

$$L_c = 2^{1/2} (\pi/\lambda) \quad , \tag{3.10}$$

or

$$L_c = [(\Delta z) \pi (2\sigma)^{1/2}] / f_0 \quad . \tag{3.11}$$

Since $\beta = 0$, the criteria for instability does not depend on the magnitude of the basic state "thermal wind" (V_T). All wavelengths longer than L_c are unstable even for very small vertical shear.

Any wave longer than this critical wavelength will amplify at the growth rate (α) where

$$\alpha = k c_i \quad . \tag{3.12}$$

The e-folding growth time is simply the inverse of α. Note that α depends on V_T and σ, and is a function of the meridional wavenumber, k. It is a maximum at an intermediate wavenumber ($0 < k^2 < 2\lambda^2$).

Table 4 shows the inverse Rossby radius of deformation, the critical wavelength (L_c), the basic state "thermal wind", and the most unstable wavelength (L_m) with its associated e-folding time for experiments 1-4 and for an imposed, unstable baroclinic jet experiment (BCJET) from a previous flat bottom study (Batteen *et al.*, 1985). In this analysis, the computations were made using the time (days 81-90), zonal (within 150 km of the eastern boundary), and meridionally averaged data from the PE model experiments.

The e-folding times for all of the experiments, at the most unstable wavelengths, are very comparable. The computed values of the e-folding times are only an approximation to the true baroclinic growth rate due to the simple two-layer baroclinic instability model used, and therefore the difference in e-folding time between all of the experiments is probably negligible.

TABLE 4

TWO-LAYER BAROCLINIC MODEL RESULTS

exp.	λ^{-1}(km)	L_c(km)	V_T (cm/s)	L_m (km)	α^{-1} (days)
#1	16.96	75.3	12	115.3	2.79
#2	16.96	75.3	8.5	115.3	3.94
#3	17.14	76.1	11	116.1	3.08
#4	16.39	72.8	8	112.8	4.05
BCJET	10.9	48.4	5.5	78.4	3.92

The short e-folding time, however, would indicate that eddy development should be apparent after about a week or so of model integration ,once this unstable state had been achieved. Indeed, eddy generation was apparent in the experiment with the imposed baroclinic jet after about 25 days of model integration. Notice that there is a large difference in the critical wavelength and associated Rossby radius of deformation between experiments 1-4 and the imposed baroclinic jet experiment. Possibly the reason eddies have not been generated in the wind-forced experiments lies in the difference between critical wavelengths.

Figure 3.21 is a plot of the e-folding times as a function of meridional wavelength ($L = 2\pi k$) for the imposed baroclinic jet experiment and experiments 1-4. The two-layer baroclinic model was applied over a ten-day averaged period of model days 81-90. The difference in critical wavelengths is readily apparent in the figure. Additionally, the most unstable wavelength is $\sim$ 80 km in the imposed baroclinic jet experiment versus $\sim$ 115 km in the windforced experiments.

To determine the baroclinicity of the experiments throughout the spin-up period, ten-day averages were computed and the two-level baroclinic model was applied for three different periods in experiment 1. Figure 3.22 shows this progression and it is clear that the baroclinic flow in this experiment is becoming more unstable throughout model spin-up. At days 21-30 the shorter wavelengths had a definite preferred growth rate while at days 81-90, the longer wavelengths are not considerably less unstable than

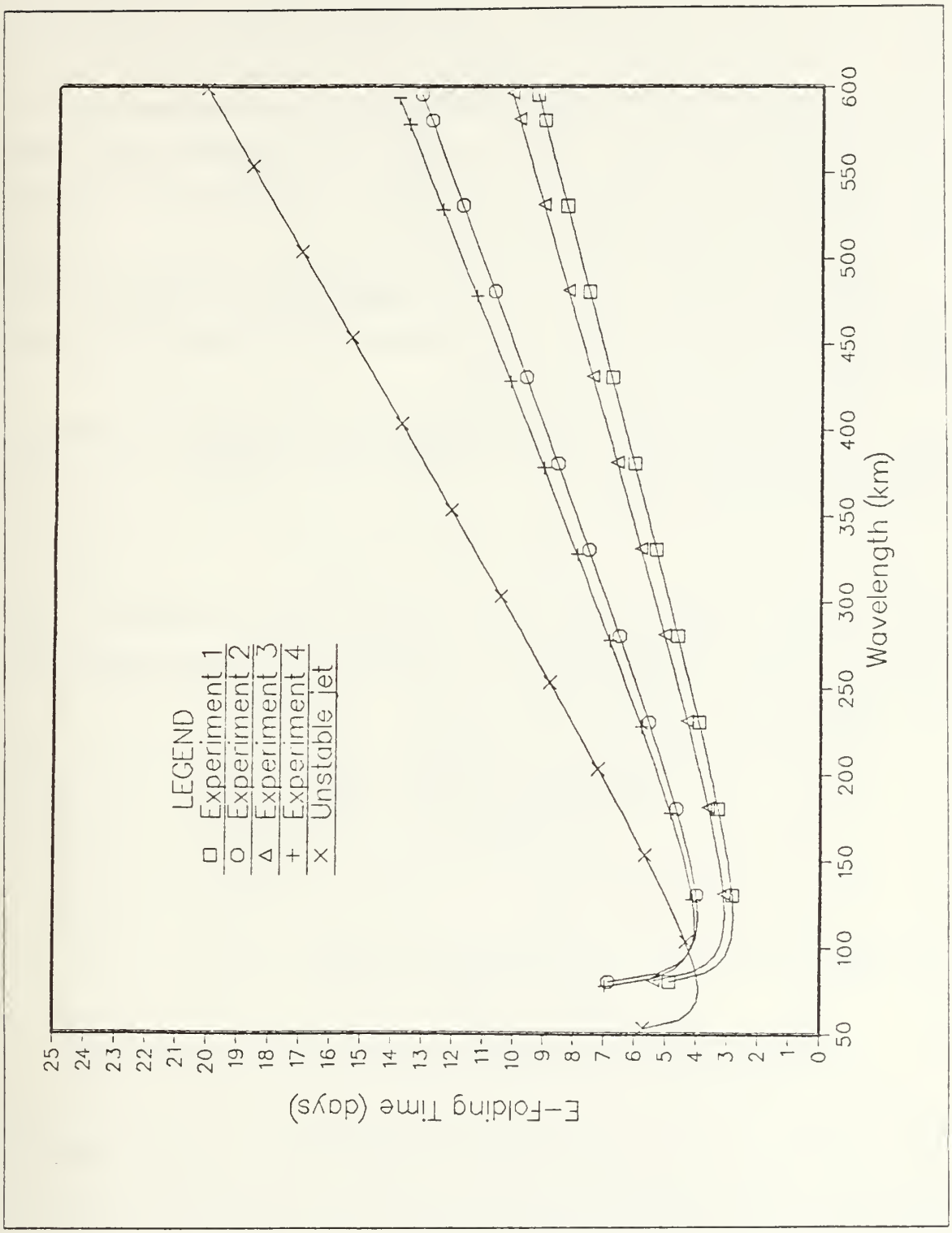

Figure 3.21 Baroclinic instability growth rates for all experiments.

the shorter wavelengths. Superimposed on Figure 3.22 is the familiar result from the imposed baroclinic jet experiment. This figure seems to imply that if the experiments were continued eddies may be generated. The problem with model continuation is that the desired realism would be lost. Re-design of model spin-up would be required including time variant wind forcing and variable parameterization of surface heat fluxes to simulate conditions indicative of the fall season. Possibly, the best solution would be to simulate an annual cycle to spin the model up. Additional computer resources would be required for an experiment of that scale.

Once a stability analysis of the mean flow is completed, it is necessary to examine model heat and momentum diffusion and its associated damping (e-folding) time. If the damping time is on the order of the growth rate for the unstable wavelengths, instability of the mean flow will be suppressed.

The PE model used in this study incorporates biharmonic heat and momentum diffusion. Following Holland and Batteen (1986), the QG baroclinic mode vorticity and thermal equation has the form:

$$(\nabla^2 - \lambda^2)\,\psi_t = \ldots - A\,\nabla^6\psi + \lambda^2 B\,\nabla^4\psi \quad , \tag{3.13}$$

where ψ is QG "temperature" (ψ_1-ψ_3 in two-layer model), A is biharmonic eddy viscosity, B is biharmonic eddy diffusion, λ is inverse Rossby radius (as before), and only the damping terms are kept in (3.13).

Assuming wave numbers (k, l), (3.13) becomes:

$$\psi_t = - \left[\frac{A(k^2 + l^2)^3 + \lambda^2 B(k^2 + l^2)^2}{k^2 + l^2 + \lambda^2} \right] \psi \quad , \tag{3.14}$$

or

$$\psi = \psi_0\, e^{-\gamma t} \quad . \tag{3.15}$$

The damping (e-folding) time of baroclinic modes is therefore

$$\gamma^{-1} = \frac{(k^2 + l^2 + \lambda^2)}{A(k^2 + l^2)^3 + \lambda^2 B(k^2 + l^2)^2} \quad . \tag{3.16}$$

Table 5 shows damping rates (γ^{-1}) and time scales γ for various wavelengths using values of $A = B = 2 \times 10^{17}$ cm^4 s^{-1} as in the PE model. It can be seen that for the most unstable wavelengths predicted by the two-layer baroclinic model for experiments 1-4 ($\sim$ 100 km), the damping time scale is $\sim$ 95 days. Since the

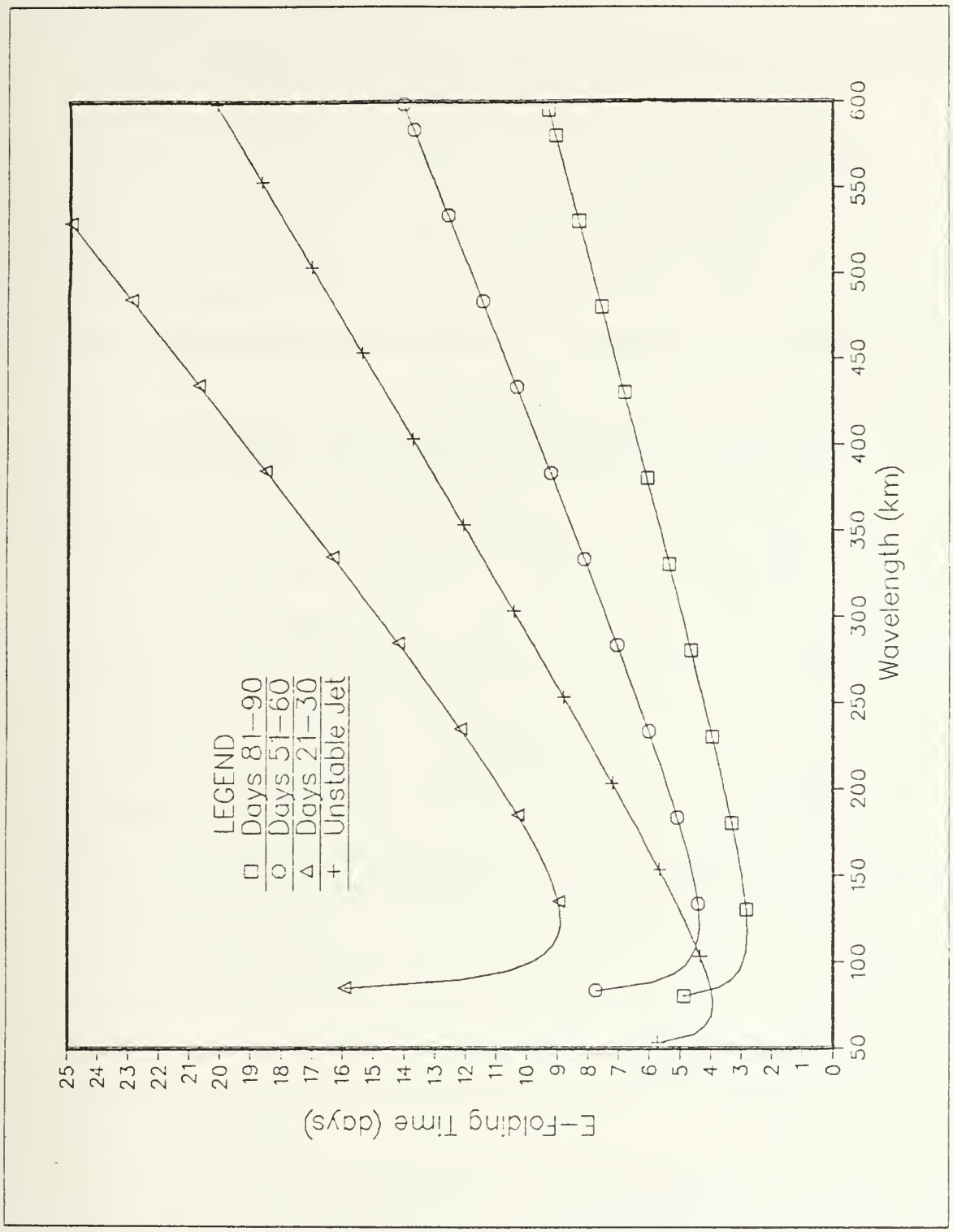

Figure 3.22 Same as Figure 3.21 except shows progression of growth rates for experiment 1.

baroclinic instability e-folding time was previously shown to be ~ 3-4 days, diffusive damping would appear to be negligible at that wavelength compared with the baroclinic growth rate. For longer wavelengths, which also have small e-folding times due to baroclinic instability, the diffusive damping is entirely negligible.

TABLE 5

DAMPING RATES FOR VARIOUS WAVELENGTHS IN THE PE MODEL

L (km)	γ (days^{-1})	γ^{-1} (days)
10	1.11×10^{2}	.009
20	0.67×10^{1}	.15
40	4.17×10^{-1}	2.4
80	2.63×10^{-2}	38
100	1.08×10^{-2}	93
200	6.76×10^{-4}	1480

IV. COMPARISON OF MODEL RESULTS WITH OBSERVATIONS

A. HISTORICAL NOTES ON THE CALIFORNIA CURRENT SYSTEM

A review and synthesis of existing literature on the CCS through 1978 is presented by Hickey (1979). Throughout the history of observations in the CCS, a set of names have been assigned to the various poleward and equatorward flows of the CCS. The California Current is the equatorward flow; the California Undercurrent refers to poleward flow over the slope; the Davidson Current is the poleward flow north of Point Conception during fall and winter; and the Southern California Countercurrent refers to the poleward flow south of Point Conception in the California Bight (Hickey, 1979). Hickey (1979) points out that as our sampling resolution increases, confusion in terminology arises and that: "The confusion in nomenclature parallels a growing uncertainty about the temporal and spatial variability of the various currents and the dynamical relationships among them." The decade following 1978 has yet to provide clear-cut definitions of the structure of the CCS and has only helped to complicate the picture by demonstrating that the CCS is more variable, both spatially and temporally, than previously thought.

Regardless of the complex variability, the flow which has been denoted the California Current generally has both an offshore and a nearshore maximum in its alongshore component. The large scale equatorward flow is believed to be fed by the northern limb of the North Pacific gyre (the West Wind Drift). This large scale alongshore component of southward flow has been observed to exceed distances of 500 km offshore in some locations. The nearshore maximum, or coastal jet, escaped attention in early studies of the CCS primarily because the majority of hydrographic data had station spacing of about 50 km. Recently, however, the emphasis has shifted to conducting surveys of finer resolution in an attempt to resolve the synoptic-mesoscale structure of the coastal jet and its associated meanders, seaward jets, and eddies.

In this study of wind forcing experiments in the CCS, the large-scale component of equatorward flow associated with the North Pacific Gyre has not been included. The experiments were conducted with an open boundary regional model with local wind forcing and for clarity of interpretation, large scale gyre circulation was neglected.

In future developments of this model, it may become necessary to include large scale gyre circulation in the quest for realistic simulations of the CCS. For the above reasons, only observations of the coastal jet and its associated undercurrent will be used for comparison with model results.

B. THE COASTAL JET

In Chapter III, the model spin-up phase was described in detail. That description was based on classical, two-dimensional coastal upwelling processes. The resultant coastal jet has been a prominent feature in descriptions of shelf circulation in the Pacific Northwest during the upwelling season (Hickey, 1979). Actual descriptions of the coastal jet, however, indicates that it varies widely in space and time. Recently, hydrographic and XBT surveys have demonstrated that instantaneous cross-sections of the California coastal region show great variability. Kosro (1986) concluded that synoptic maps of near-surface currents off northern California deviated substantially from the classical description of two-dimensional wind driven upwelling. Huyer and Kosro (1986) conducted six surveys near Point Arena, California during the upwelling season in 1981 and 1982. The simple two-dimensional, equatorward baroclinic coastal jet was observed during only one of the six surveys (20-22 April 1982). The simple two-dimensional coastal jet is almost invariably resolved in the averaged velocity fields off California during the upwelling season. Huyer and Kosro (1986) found that the average velocity fields (computed over all 6 surveys) consistently showed baroclinic, equatorward flow in the upper layers and weak poleward flow along the shelf-break at a depth of $\sim$ 150 m. Additionally, it was noted that the eddies and meanders which dominated the velocity field during most surveys were absent from the average field. All of their surveys revealed a baroclinic equatorward jet which wound around eddies and at times turned directly offshore. It is hypothesized that since the classical form of the coastal jet appears in the average velocity fields, but only rarely in a synoptic survey, the upwelling induced coastal jet becomes unstable off northern California during the upwelling season.

The classical two-dimensional coastal jet is somewhat more prevalent in its pure form off the coast of Oregon. In two successive years (1965 and 1966), the frontal zone of the coastal upwelling region off Oregon was studied by Mooers *et al.* (1976). They found that the computed velocity field showed equatorward surface flow and a poleward undercurrent below the inclined frontal layer. Both the southward surface

flow and the northward undercurrent exhibited a "jet-like structure." The southward jet was most intense ($\sim$ 20 cm/s) within 20 km from the shore and in the upper 40 m. The poleward undercurrent was most intense ($\sim$ 10 cm/s) between 10 and 40 km offshore and at a depth of 80 to 200 m.

Huyer and Kosro (1986) state that, as previously discussed, a baroclinic coastal jet was manifested in classical form during their 20-22 April 1982 survey off northern California. The strength and position of the jet's core (over the shelf-break) were nearly uniform over the entire alongshore extent of the survey region ($\sim$ 100 km). This anisotropic characteristic (more rapid variation cross-shore than alongshore) is a recurrent feature of the coastal jet in its stable form. The coastal jet was further characterized by a clearly defined core located about 25 km from the coast with southward velocities > 50 cm/s at 20 m depth. Increasing in depth to 80 m, the core was located farther from shore ($\sim$ 40 km) with maximum southward velocities less than 30 m/s. Available data suggested that there existed a narrow (10-20 km) poleward undercurrent at $\sim$ 150 m depth with maximum velocities of about 15 cm/s.

Strong horizontal and vertical shear is a persistent characteristic of the baroclinic coastal jet. Huyer (1983) found the maximum vertical shear to be relatively constant ($\sim 4 \times 10^{-3}$ s^{-1}) during the upwelling season in spite of significant wind stress fluctuations. Huyer and Kosro (1986) used current meter data to determine that average maximum vertical shear was $4\text{-}5 \times 10^{-3}$ s^{-1} in the upper 35 m over the outer shelf during the 1981 and 1982 surveys. Kosro (1986) computed vertical shear to be greater than 2×10^{-3} s^{-1} in the coastal jet off northern California during CODE with observed cyclonic horizontal shear exceeding 10^{-4} s^{-1} which is the local value of the Coriolis parameter (f). Mooers *et al.* (1976) computed mean geostrophic vertical shear from the thermal wind equation to be $\sim 4 \times 10^{-3}$ s^{-1} off Oregon which compared well with their measured current shear of 4.6×10^{-3} s^{-1} in the coastal jet off Oregon. Kosro and Huyer (1986) collected data across a seaward jet off northern California and suggested that it was continuous with the coastal jet. Horizontal shear on the cyclonic side of the jet was estimated to be on the order of 10^{-4} s^{-1} (f) and on the order of f/3 or less for the anticyclonic side of the jet.

C. COMPARISONS

The most important consideration in a comparison of model results with observations is which model assumptions might cause the model results to deviate most

significantly from nature. In this study there are two rather artificial assumptions, the flat-bottom and the straight coastline, which could significantly alter the results from that observed in nature. As discussed in Chapter II, however, the flat-bottom and straight coastline are crucial in interpretation of early modeling results. It is with this in mind that the following comparisons are presented. Table 6, below, is a synopsis of some of the more interesting features of the coastal jet generated in experiments 1-4 along with generalized features of a classical, upwelling-induced, two-dimensional coastal jet occasionally found off the coast of northern California and Oregon.

TABLE 6

STATISTICAL COMPARISON OF MODEL RESULTS WITH OBSERVATIONS OF THE COASTAL JET

	exp.1	exp.2	exp.3	exp.4	obs.
A.	100 cm/s	75 cm/s	100 cm/s	70 cm/s	30-50 cm/s
B.	25 km	25 km	25 km	25 km	~25 km
C.	20 km	20 km	28 km	28 km	~35 km
D.	100 km	190 km	100 km	190 km	25-100 km
E.	1000 m	1000 m	1000 m	1000 m	< 100 m
F.	5-10 cm/s	5-10 cm/s	5-10 cm/s	5-10 cm/s	5-15 cm/s
G.	60 km	25 km	50 km	20 km	~15 km
H.	2.8 s^{-1}	2.6 s^{-1}	2.9 s^{-1}	2.6 s^{-1}	2-5 s^{-1}
I.	.15f	.1f	.6f	.4f	~f/2
J.	-.2f	-.15f	-.2f	-.15f	~-f/3
K.	.07 °/km	.05 °/km	.06 °/km	.05 °/km	~.05 °/km
L.	8.5 °C	9.5 °C	9.0 °C	10.0 °C	12-13 °C

The letter designations in Table 6 have the following meanings:

A. Maximum jet velocity.
B. Offshore location of surface jet axis.
C. Offshore location of depth averaged jet axis.
D. Offshore extent of jet.
E. Depth of jet.
F. Maximum undercurrent velocity.
G. Width of undercurrent.
H. Maximum vertical shear ($\times 10^{-3}$).
I. Maximum horizontal cyclonic shear.
J. Maximum horizontal anticyclonic shear.
K. Nearshore surface temperature gradient.
L. Mean coastal surface temperature.

The maximum jet velocities that developed in experiments 1-4 exceed the observed values by about a factor of two. The exceptionally strong surface currents developed in experiments 1 and 3 may be explained in part by the unrealistically large value of wind stress at the coast in those experiments. The surface stress values were chosen by taking an offshore mean climatological value and applying it uniformly across the model domain. Experiments 2 and 4, which included the curl of wind stress, had more realistic (reduced) values of wind stress near the coast and indeed produced more realistic surface currents. Additionally, winds were input as steady which may produce stronger currents than a time varying forcing function. Time variable winds may by a key to generating instabilities in the coastal jet and thus limiting its growth. Note that experiment 4 produced the maximum jet velocities closest to those observed.

The offshore location of the jet axis, at the surface and with depth, compared favorably with observed locations. The vertical structure of the coastal jet tends to follow the coastal slope. The vertical eastern boundary in the model produced an almost vertically stacked jet, whereas the slope off northern California produces a coastal jet which tilts offshore with depth. Associated with the axis location is the offshore extent of the jet. Observations indicate that the coastal jet is a narrow feature which extends horizontally offshore from 25-100 km. Experimental results show a coastal jet about 100 km wide. The inclusion of wind stress curl (experiments 2 and 4) tended to increase the width of the modeled equatorward flow but the main body of the jet remained about 100 km in width.

The depth of jet penetration in the water column is by far the largest deviation of model results from observations. Further experimentation and analysis is needed to identify the cause of this major discrepancy. One possibility is the absence of a shelf slope topography in the model. Model basin depth is constant at 4500 m which means that the coastal jet penetrated to about one-fourth of the basin depth. Observations show that the observed coastal jet penetrates to about one-third of the continental shelf depth. Therefore a relative comparison of model results with observations is good. Preliminary results of a wind forcing experiment with idealized cross-shore topography indicates that the model coastal jet penetration is in fact dependent on shelf depth. An additional consideration in the vertical structure of the jet is the vertical temperature stratification. McCreary *et al.* (1986) suggests that a shallow ($\sim$ 100 m) seasonal thermocline may be very important in the formation of the coastal jet, whereas the model's basic stratification was that corresponding to the major thermocline having a vertical scale of 450 m.

The poleward undercurrent maximum velocities in experiments 1-4 were somewhat slow as compared with observations and also seem independent of the magnitude of wind stress. Topography, again, may be an important mechanism in the formation of undercurrents. Open boundary conditions in the model may modify the formation of an undercurrent as compared with the effects of gyre scale circulation in the North Pacific. Wind relaxation events off the coast of California have also been considered to be closely associated with undercurrents and countercurrents within the CCS. Mooers *et al.* (1976) stated that "The relationship between the northward Davidson Inshore Current, the California Countercurrent, and the undercurrent associated with coastal upwelling is not understood." It is probably safe to say that that statement still holds true today. Recent emphasis in the oceanographic community has been placed on efforts to understand those relationships. The width of the undercurrent is generally considered very narrow ($\sim$ 15 km), as described by Huyer and Kosro (1986). Experiment 4 produced the narrowest undercurrent (20 km) which corresponds well with observations.

Vertical and horizontal shear measurements have demonstrated that the coastal jet off California and Oregon is a highly sheared system. Values for the vertical shear range from about 2×10^{-3} s^{-1} to 5×10^{-3} s^{-1} (Huyer, 1983; Kosro, 1986; Mooers *et al.*, 1986). Experimental shear values fall within that range but on the low side ($\sim$ 3×10^{-3} s^{-1}). The topographic influence may again be important to the establishment

of large vertical shear. The coastal shelf and slope, in compressing the vertical structure of the jet, may also increase the associated vertical shear. The measurements of horizontal shear in the CCS suggest that a typical value for the cyclonic shear may be on the order of f/2 to f and that the anticyclonic shear is on the order of -f/3 (Kosro, 1986). Experimental results demonstrate that a free-slip boundary condition on the eastern boundary (experiments 1 and 2) prevents the development of large horizontal cyclonic shear. Even with the zero-slip boundary condition (experiments 3 and 4) the largest cyclonic shear developed by the PE model was .6f. Anticyclonic shear was similarly smaller in the model experiments than the observed values of $\sim$-f/3.

Of course, the coastal temperature structure is closely tied to the coastal jet structure owing to its baroclinic nature. The observed offshore surface temperature gradient during the upwelling season off northern California is on the order of .05 °/km with a mean July coastal temperature of 10-13 °C (Huyer and Kosro, 1986). Model results show a range of gradients of .05-.07 °/km with coastal temperatures in the range of 8.5-10 °C. Those values compare well, and the cooler model coastal temperatures may be explained by the unrealistically high model jet velocities or inexact surface heat flux parameterization.

It is difficult to make a quantitative comparison of experimental results with observations of the coastal jet in the CCS. Observed values of jet characteristics vary widely from study to study and the stable form of the classical two-dimensional coastal jet has been infrequently surveyed. From the above discussion, it is clear that the structure of the simulated coastal jet is sensitive to the forcing function, boundary conditions, heating parameterization, topography, and a host of other conditions too numerous and complex for the scope of this study. Experiment 4, which included idealized, climatological wind stress curl with a zero-slip boundary condition on the eastern boundary, was the best simulation of the coastal jet of the four experiments conducted in this study.

V. SUMMARY AND CONCLUSIONS

A. SUMMARY

This study has examined the response of an idealized, flat-bottom, eastern boundary oceanic regime to steady, equatorward, local wind-forcing on a seasonal time scale. Both uniform and offshore-varying wind, with zero-slip and free-slip boundary conditions on the eastern boundary, were employed as forcing mechanisms in a ten-level, high resolution, primitive equation ocean model.

A classical two-dimensional, upwelling-induced, equatorward flowing coastal jet, with an associated poleward undercurrent, developed in response to both uniform and offshore-varying wind forcing. The variations in formation and structure of the coastal jet and undercurrent were explored and analyzed in four numerical experiments: uniform wind with free-slip; offshore-varying wind with free-slip; uniform wind with zero-slip; and offshore-varying wind with zero-slip.

1. Stability Analysis

Instability of the mean flow did not occur in any of the aforementioned experiments and, therefore, eddies did not develop. A stability analysis was conducted on all of the modeled coastal jets in this study along with an imposed coastal jet from a previous, unforced, flat-bottom experiment (Batteen *et al.*, 1985) which formed eddies after approximately thirty days of model run time. Potential vorticity was computed throughout the model domain of each experiment and the cross-stream derivative of potential vorticity was found to change sign in the region of each modeled coastal jet. This fact established that the modeled coastal jets all satisfied the necessary condition for mixed (barotropic and baroclinic) instability.

To further explore conditions for instability, a two-layer, quasigeostrophic, baroclinic instability model was applied to each experiment. It was established that all of the experiments satisfied the sufficient conditions for baroclinic instability as defined by the simple two-layer stability model. The four experiments conducted in this study did not significantly vary in critical wavelengths, most-unstable wavelengths, or in baroclinic instability e-folding times. However, the imposed baroclinic jet experiment (Batteen *et al.*, 1985) had a shorter critical wavelength and a shorter most-unstable wavelength than the four wind-forced experiments. The e-folding rates for longer

wavelengths were somewhat larger in the imposed baroclinic jet experiment as compared with this study's experiments; which would indicate that the wind-forced jets are more unstable than the imposed jet at longer wavelengths. The reason why instability of the mean flow did not occur in the model generated coastal jets remains an open scientific question.

2. **Comparison with Observations**

A comparison of model results with observations of the CCS was conducted. A numerical model can properly simulate nature only to the extent which observations have provided the modeler with understanding of the feature he desires to simulate. This is a problematic area in modeling the CCS. Observations of the CCS demonstrate great variability in time and space and the classical two-dimensional upwelling-induced coastal jet has been infrequently observed and studied off California. With this in mind, a synthesis of literature addressing the coastal jet was conducted and a range of values for some of the more important characteristics was compiled and compared with model results.

The model generated coastal jet compared favorably with observations in offshore axis location, undercurrent strength and width, vertical and horizontal shears and surface temperature gradients. Some deficiencies were noted. These included discrepancies in the strength, depth, and offshore extent of the modeled coastal jet compared with observations. Experiment 4, which included wind stress curl with a zero-slip boundary condition, is believed to be the most realistic model jet produced in this study.

3. **Effects of Offshore Varying Wind Forcing**

Positive wind stress curl, within 200 km of the eastern boundary, was applied by the offshore-varying wind forcing in two of the experiments (experiments 2 and 4). The positive wind stress curl induced cyclonic relative vorticity to the system and added an additional component of upwelling, due to the effect of Ekman pumping, to the coastal upwelling component (caused by equatorward wind forcing along the eastern model boundary). The Ekman pumping induced upward vertical motion, from surface divergence, within 200 km of the coast and created an extended zone of baroclinicity in the upper layers of the ocean. The extended zone of baroclinicity, therefore, increased the width of equatorward flow over that generated by the experiments with uniform wind forcing (experiments 1 and 3). Positive wind stress curl near the coast also moved the depth-averaged jet axis, along with the undercurrent axis, farther offshore than forcing without curl.

4. Effects of the Zero-Slip Boundary Condition

As previously discussed, both free-slip and zero-slip boundary conditions were employed on the eastern model boundary. The free-slip boundary condition implies that the offshore gradient of tangential velocity vanishes at the boundary (experiments 1 and 2), and the zero-slip condition sets the tangential velocity itself to zero at the coast (experiments 3 and 4). The zero-slip boundary condition, therefore, imparted cyclonic relative vorticity to the inshore side of the model coastal jet. From the comparison of model results with observations of the CCS, it is believed that eastern boundary coastal circulation is best simulated, in a high resolution model, with the use of a zero-slip boundary condition on the eastern boundary.

B. RECOMMENDATIONS

This study was a first step in a numerical modeling effort at the Naval Postgraduate School in implementing wind forcing into a PE model designed to simulate the CCS off northern California. It is important for future studies to determine the reasons why instability of the mean flow produced by wind-forcing, in this study, does not occur when stability analyses indicates that the flow is unstable. The development and evolution of eddies observed in the CCS is of extreme interest, and understanding instability of the mean flow may be the key to understanding eddy processes. Designing future experiments to understand the vertical structure of the jet and why the model jet is much stronger and wider than the observed coastal jet should be given high priority as well.

This study had the constraint of a flat-bottom basin with a regular coastline. Implementation of topography first requires the addition of depth-averaged flow within the PE model for scientific validity. Once the depth-averaged flow is incorporated, the door will be opened for a series of studies of wind-forced circulation over idealized topography. The influence of topography is thought to have a great impact on coastal circulation. Additionally, an irregular coastline which would simulate capes and bays along the coast of California would be a fascinating study.

Finally, one should consider the inclusion of gyre-scale circulation as the baseline for wind-forcing experiments in the CCS. The gyre-scale circulation could be used to initialize the model prior to model spin-up by local wind-forcing. Time-dependent winds could eventually be investigated as the prelude to model forcing by actual, observed wind records.

APPENDIX

ANALYTIC APPROXIMATION OF UPWELLING TIME SCALE

The time scale over which upwelling occurs may be analytically approximated through use of the principle of conservation of mass, scale analysis, and Ekman transport. The upwelling rate can then be compared with the PE model results for verification of model physics. The approximation involves no diabatic heating and neglects the component of velocity due to pressure gradient force. A control experiment was conducted which included no diabatic processes (surface thermal damping) and which had uniform, steady wind forcing. That experiment will be used for comparison with the following approximation. All symbols, in the following derivation, are as defined in Chapter II unless otherwise stated.

To arrive at a scale for the vertical component of velocity, the equation of continuity, with the assumption of incompressibility, is written as

$$\frac{\partial u}{\partial x} + \frac{\partial v}{\partial y} + \frac{\partial w}{\partial z} = 0 \quad . \tag{A.1}$$

Assuming no longshore variation in v, then equation (A.1) may be reduced to

$$\frac{\partial u}{\partial x} + \frac{\partial w}{\partial z} = 0 \quad . \tag{A.2}$$

Scale analysis of equation (A.2) yields the following scale for w (vertical velocity):

$$W \sim \frac{U H}{L_x} \quad , \tag{A.3}$$

where UH is mass transport and L_x is a length scale.

Since it is desired to isolate the effect of upwelling caused only by motion of the fluid away from the solid boundary driven by surface stress, Ekman mass transport (M_E) is required where

$$M_{Ex} \equiv \int_{-H}^{0} \rho_o u_E \, dz = \frac{\tau_y}{f} \quad ,$$

which may be rewritten as

$$\frac{\tau_y}{f} = \rho_o U H \quad ,$$

or

$$U H = \frac{\tau_y}{\rho_o f} \quad . \tag{A.4}$$

Using equation (A.3), W is substituted into equation (A.4) to arrive at the following relationship between vertical velocity and surface stress:

$$W \sim \frac{\tau_y}{\rho_o f L_x} \quad . \tag{A.5}$$

The surface stress can be calculated, through use of the bulk aerodynamic formula with a constant drag coefficient, by

$$\tau_y = \rho_a C_D V^2 \quad .$$

Substituting this expression for τ_y into equation (A.5) results in the final form for vertical velocity (W) of

$$W \sim \frac{\rho_a C_D V^2}{\rho_o f L_x} \quad . \tag{A.6}$$

Using a value of V = 900 cm s^{-1} and L_x = 14.2 km (the second internal Rossby radius of deformation computed by the method of Feliks (1985)), equation (A.6) yields a scale value for the vertical velocity, generated by coastal upwelling, of

$$W \sim 0.00947 \text{ cm/sec} = 8.18 \text{ m/day}.$$

Model output demonstrates that, in the upper levels of the ocean, vertical velocity decreases by 80-90% within two gridpoints of the coast. This length scale, of 16 km, compares well with the second internal Rossby radius of deformation. The model length scale of vertical velocity does not, however, compare well with the first Rossby radius of deformation which was computed to be 29.3 km. The horizontal length scale corresponding to the second Rossby radius of deformation is appropriate because the model vertical velocity has a maximum close to the sea-surface.

A comparison of the rate of model upwelling with that obtained from an Ekman balance was also made starting, arbitrarily, at model day 30 since Ekman balance is not well established during the initial days of model spin-up. At this time, the depth of the 9.03° C isotherm (chosen for illustrative purposes) at the coast was 169.4 m (level 4).

Using the vertical velocity approximation computed above, the 9.03° C isotherm should be displaced to level 1 (12.9 m) in 20.65 days. Model output demonstrates that, at day 50.65, coastal temperature at level 1 is 9.19° C which compares quite favorably with the analytically approximated temperature of 9.03° C.

LIST OF REFERENCES

Anderson, D.L.T., and A.E. Gill, 1975: Spin-up of a stratified ocean with applications to upwelling. *Deep Sea Res.*, **22**, 583-596.

Arakawa, A., and V.R. Lamb, 1977: Computational design of the basic dynamical processes of the UCLA general circulation model. *Methods in computational Physics*, J. Chang. Ed., Academic Press, **17**, 173-265.

_____, and M.J. Suarez, 1983: Vertical differencing of the primitive equations in sigma coordinates. *J. Atmos. Sci.*, **111**, 34-45.

Batteen, M.L., R.L. Haney and C.N.K. Mooers, 1985: Coastal and bathymetric influences on eddy generation in the California Current System. IAMAP/IAPSO Joint Assembly, Honolulu, Hawaii, 5-16 August.

Blandford, R.R., 1971: Boundary conditions in homogeneous ocean models. *Deep-Sea Res.*, **18**, 739-751.

Blumberg, A.F., L.H. Kantha, H.J. Herring and G.L. Mellor, 1984: California shelf physical oceanography circulation model. Final Report No. 88, Dynalysis of Princeton, Princeton, NJ.

Bryan, K., 1963: A numerical investigation of a nonlinear model of a wind-driven ocean. *J. Atmos. Sci.*, **20**, 594-606.

_____, and P. Ripa, 1978: The vertical structure of North Pacific temperature anomalies. *J. Geophys. Res.*, **83**, 2419-2429.

Camererlengo, A.L., and J.J. O'Brien, 1980: Open boundary conditions in rotating fluids. *J. Comput. Physics.*, **35**, 12-35.

Carton, J.A., 1984: Coastal circulation caused by an isolated storm. *J. Phys. Oceanogr.*, **14**, 114-124.

_____, and S.G.H. Philander, 1984: Coastal upwelling viewed as a stochastic process. *J. Phys. Oceanogr.*, **14**, 1499-1509.

Chelton, D.B., 1984: Seasonal variability of alongshore geostrophic velocity off central California. *J. Geophys. Res.*, **89**, 3473-3486.

Feliks, Y., 1985: Notes and correspondence on the Rossby radius of deformation in the ocean. *J. Phys. Oceanogr.*, **15**, 1605-1607.

Gill, A.E., 1982: *Atmosphere-Ocean Dynamics.* Academic Press, 662 pp.

Haltiner, G.J., and R.T. Williams, 1980: *Numerical Prediction and Dynamic Meteorology*, 2nd edition, John Wiley and Sons Inc., 477 pp.

Haney, R.L., 1971: Surface thermal boundary condition for ocean circulation models. *J. Phys. Oceanogr.*, **1**, 241-248.

_____, W.S. Shiver and K.H. Hunt, 1978: A dynamical-numerical study of the formation and evolution of large-scale ocean anomalies. *J. Phys. Oceanogr.*, **8**, 952-969.

_____, 1985: Midlatitude sea surface temperature anamolies: A numerical hindcast. *J. Phys. Oceanogr.*, **15**, 787-789.

Hickey, B.M., 1979: The California Current System - hypothesis and facts. *Prog. in Oceanogr.*, **8**, 191-279.

Holland, W.R., and M.L. Batteen, 1986: The parameterization of subgrid-scale heat diffusion in eddy-resolved ocean circulation models. *J. Phys. Oceanogr.*, **16**, 200-206.

Holton, J.R., 1979: *An Introduction to Dynamic Meteorology*, 2nd edition, Academic Press, 391 pp.

Huyer, A., 1983: Coastal upwelling in the California Current System. *Prog. in Oceanogr.*, **12**, 259-284.

_____, and P.M. Kosro, 1986: Mesoscale CTD and velocity surveys over the shelf and slope in the upwelling region near Pt. Arena, California. Submitted to *J. Geophys. Res.*

Kosro, P.M., 1986: CTD and velocity surveys of seaward jets off northern California, July 1981 and 1982. *J. Geophys. Res.*, 91, 7680-7690.

_____, and Huyer A., 1986: Structure of the coastal current field off northern California during CODE. Submitted to *J. Geophys. Res.*

Large, W.G., and S. Pond, 1981: Open ocean momentum flux measurements in moderate to strong winds. *J. Phys. Oceanogr.*, 11, 324-336.

List, R.J., 1963: *Smithsonian Meteorological Tables.* Smithsonian Institution, Washington, DC, 527 pp.

McCreary, J.P., Jr., P.K. Kundu and S.-Y. Chao, 1986: Dynamics of the California Current System. Submitted to *J. Mar. Res.*

Miller, D.B., and R.G. Feddes, 1971: *Global Atlas of Relative Cloud Cover*, 1967-1970. U.S. Dept. of Commerce, NOAA, NESS, and U.S. Air Force, Washington, DC, 237 pp.

Mooers, C.N.K., C.A. Collins and R.L. Smith, 1976: The dynamic structure of the frontal zone in the coastal upwelling region off Oregon. *J. Phys. Oceanogr.*, 6, 3-21.

_____, and A.R. Robinson, 1984: Turbulent jets and eddies in the California Current and inferred cross-shore transports. *Science*, **223**, 51-53.

Nelson, C.S., 1977: Wind stress and wind stress curl over the California Current. *NOAA Tech. Rep. NMFS SSRF-714*, U.S. Dep. Commer., 87 pp.

_____, and D.M. Husby, 1983: Climatology of surface fluxes over the California Current region. *NOAA Tech. Rep. NMFS SSRF-763*, U.S. Dep. Commer., 155 pp.

Philander, S.G.H., and J.-H. Yoon, 1982: Eastern boundary currents and coastal upwelling. *J. Phys Oceanogr.*, **12**, 862-879.

Robinson, A.R., 1983: *Eddies in Marine Science*, Springer-Verlag, New York, 609 pp.

Thomson, R.E., 1984: A cyclonic eddy over the continental margin of Vancouver Island: Evidence for baroclinic instability. *J. Phys. Oceanogr.*, 14, 1326-1348.

Veronis, G., 1966: Wind-driven ocean circulation: Part II. Numerical solutions of the non-linear problem. *Deep-Sea Res.*, 13, 31-55.

INITIAL DISTRIBUTION LIST

		No. Copies
1.	Defense Technical Information Center Cameron Station Alexandria, VA 22304-6145	2
2.	Library, Code 0142 Naval Postgraduate School Monterey, CA 93943-5002	2
3.	Chairman (Code 58Tm) Department of Oceanography Naval Postgraduate School Monterey, CA 93943	1
4.	Chairman (Code 63Rd) Department of Meteorology Naval Postgraduate School Monterey, CA 93943	1
5.	Dr. R.L. Haney (Code 63Hy) Department of Meteorology Naval Postgraduate School Monterey, CA 93943	2
6.	Dr. M.L. Batteen (Code 68Bv) Department of Oceanography Naval Postgraduate School Monterey, CA 93943	2
7.	Dr. C.N.K. Mooers (Code 68Mr) Department of Oceanography Naval Postgraduate School Monterey, CA 93943	1
8.	Dr. D. Smith (Code 68Si) Department of Oceanography Naval Postgraduate School Monterey, CA 93943	1
9.	Lt Philip G.Renaud 88 Read St. Somerset, Ma 02726	2
10.	Director Naval Oceanography Division Naval Observatory 34th and Massachusetts Avenue NW Washington, DC 20390	1
11.	Commander Naval Oceanography Command NSTL Station Bay St. Louis, MS 39522	1
12.	Commanding Officer Naval Oceanographic Office NSTL Station Bay St. Louis, MS 39522	1

13.	Commanding Officer Fleet Numerical Oceanography Center Monterey, CA 93943	1
14.	Commanding Officer Naval Ocean Research and Development Activity NSTL Station Bay St. Louis, MS 39522	1
15.	Commanding Officer Naval Environmental Prediction Research Facility Monterey, CA 93943	1
16.	Chairman, Oceanography Department U.S. Naval Academy Annapolis, MD 21402	1
17.	Naval Ocean Research and Development Activity 800 N. Quincy Street Arlington, VA 22217	1
18.	Office of Naval Research (Code 420) 800 N. Quincy Street Arlington, VA 22217	1
19.	Scientific Liason Office Office of Naval Research Scripps Institution of Oceanography La Jolla, CA 92037	1
20.	Commander Oceanographic Systems Pacific Box 1390 Pearl Harbor, HI 96860	1
21.	Commanding Officer Naval Eastern Oceanography Center Naval Air Station Norfolk, VA 23511	1
22.	Commanding Officer Naval Western Oceanography Center Box 113 Pearl Harbor, HI 96860	1
23.	Commanding Officer Naval Oceanography Command Center, Rota Box 31 FPO San Francisco, CA 09540	1
24.	Conmanding Officer Naval Oceanography Command Center, Guam Box 12 FPO San Francisco, CA 96630	1
25.	Dr. C.A. Collins Program Director Physical Oceanography National Science Foundation Washington, D.C. 20550	1

18070 2

DUDLEY KNOX LIBRARY
NAVAL POSTGRADUATE SCHOOL
MONTEREY, CALIFORNIA 93943-5002

221158

Thesis
R3356 Renaud
c.1 Wind forcing experiments in the California current system.

221158

Thesis
R3356 Renaud
c.1 Wind forcing experiments in the California current system.

thesR3356
Wind forcing experiments in the Californ
3 2768 000 76073 0
DUDLEY KNOX LIBRARY